A General Safety-Certified Cooperative Control Architecture for Interconnected Intelligent Surface Vehicles With Applications to Vessel Train

Wentao Wu, *Student Member, IEEE*, Zhouhua Peng, *Senior Member, IEEE*, Lu Liu, *Member, IEEE*, and Dan Wang, *Senior Member, IEEE*

***Abstract*—This paper considers cooperative control of interconnected intelligent surface vehicles (ISV) moving in a complex water surface containing multiple static/dynamic obstacles. Each ISV is subject to control force and moment constraints, in addition to internal model uncertainties and external disturbances induced by wind, waves and currents. A general safety-certified cooperative control architecture capable of achieving various collective behaviors such as consensus, containment, enclosing, and flocking, is proposed. Specifically, a distributed motion generator is used to generate desired reference signals for each ISV. Robust-exact-differentiators-based (RED-based) extended state observers (ESOs) are designed for recovering unknown total disturbances in finite time. With the aid of control Lyapunov functions, input-to-state safe high order control barrier functions and RED-based ESOs, constrained quadratic optimization problems are formulated to generate optimal surge force and yaw moment without violating the input, stability, safety constraints. In order to facilitate real-time implementations, a one-layer recurrent neural network is employed to solve the constrained quadratic optimization problem on board. It is proved that all tracking errors of the closed-loop system are uniformly ultimately bounded and the multi-ISV system is input-to-state safe. An example is given to substantiate the effectiveness of the proposed general safety-certified cooperative control architecture.**

***Index Terms*—Distributed motion generator, intelligent surface vehicles, input-to-state safe high-order control barrier function, one-layer recurrent neural networks.**

Manuscript received March 7, 2022; revised April 5, 2022; accepted April 16, 2022. This work was supported in part by the National Natural Science Foundation of China under Grants 51979020, 51909021, 51939001, and 52071044, in part by the Top-notch Young Talents Program of China under Grant 36261402, in part by Liaoning Revitalization Talents Program under Grant XLYC2007188, in part by the Science and Technology Fund for Distinguished Young Scholars of Dalian under Grant 2018RJ08, in part by the Basic Scientific Research in Colleges and Universities of Liaoning Provincial Education Department under Grant LJKQZ2021007, and in part by the Fundamental Research Funds for the Central Universities. *(Corresponding author: Zhouhua Peng.)*

Wentao Wu and Lu Liu are with the School of Marine Electrical Engineering, Dalian Maritime University, Dalian 116026, China, and also with the Department of Automation, Shanghai Jiao Tong University, Shanghai 200240, China (e-mail: wentao-wu@sjtu.edu.cn; luliu@dlmu.edu.cn).

Zhouhua Peng and Dan Wang are with the School of Marine Electrical Engineering, Dalian Maritime University, Dalian 116026, China (e-mail: zhpeng@dlmu.edu.cn; dwang@dlmu.edu.cn).

Color versions of one or more figures in this article are available at https://doi.org/10.1109/TIV.2022.3168974.

Digital Object Identifier 10.1109/TIV.2022.3168974

I. Introduction

With the rapid advancements in communication and computer technologies, cooperative operations of multiple intelligent vehicles has aroused plentiful interest worldwide [1]–[5]. Intelligent surface vehicles (ISV) is a marine transportation platform with numerous applications such as carriage of goods, conveying of passengers and waterway transportation [6]–[8]. A number of cooperative control approaches are proposed such as virtual structure mechanisms [9], behavioral methods [10], artificial potential fields [11], graph-based methods [12], and leader-follower approaches [13].

Various cooperative control approaches for multiple ISVs are proposed; see the references and therein [14]–[27]. Specifically, in [14], [15], leader-follower formation control methods with predefined transient properties are devised for ISVs with the ability of collision avoidance. In [16], an output-feedback consensus maneuvering control method is investigated for a fleet of ISVs, which addresses a cooperative time-varying formation maneuvering problem with connectivity preservation and collision avoidance. In [17], an output-feedback flocking control method is developed for marine vehicles based on data-driven adaptive extended state observers (ESOs). In [18], an observer-based finite-time containment control method is proposed to achieve a path-guided formation capable of avoidance collision and connectivity preservation. In [19], a distributed robust collision-free formation control scheme based on the super-twisting control and persistent excitation is developed for underactuated vessels, which may possess completely different dynamic models. In [20], an improved real-time attitude guidance scheme with the dynamical virtual ship is initially developed for the waypoints-based path-following of ISVs subject to multi-static or slow time-varying obstacles. In [21], a model-reference collision-free tracking control method is presented for surface vehicles to enhance control accuracy and intelligence by using the reinforcement learning technique. In [22], a new nonlinearly transformed formation error is constructed for ISVs to achieve the connectivity preservation, the collision avoidance, and the distributed formation without switching the desired formation pattern and using any additional potential functions. In [23], a robust leader-follower formation tracking algorithm is presented by using connectivity-maintaining and collision-avoiding performance functions for vessels with range-limited communication and completely unknown nonlinearities. In [24], the local path replanning-based repulsive potential function technique is designed to achieve the collision-free distributed formation control with the distributed fixed-time estimator. In [25], a target region tracking control strategy based on the adaptive neural network (NN) is proposed for ocean vessels without no intra-group collisions. In [26], a distributed synchronization controller based on p-times differentiable step functions is designed for multiple ISVs while ensuring no collisions among neighboring ships. In [27], an intent inference-based probabilistic velocity obstacle method is developed to avoid COLREG-violating vessels by combining the marine traffic rules with the proactive evasive actions. However, the formation control methods presented in [7]–[9], [12]–[27] are designed for specific formation scenarios with different control architectures, which may be inflexible in practice one one hand. On the other hand, the collision avoidance methods presented in [14]–[27] cannot avoid collisions with static obstacles, dynamic obstacles, and the neighboring vehicles, simultaneously.

In this paper, we present a general collision-free safety-certified cooperative control architecture for multiple interconnected ISVs subject to input constraints, model uncertainties and environmental disturbances. The cooperative control architecture includes a high-level distributed motion generator and a low-level trajectory tracking controller. Specifically, the distributed motion generator prescribes the reference trajectories for achieving desired swarm behaviors including consensus, containment, enclosing, flocking, etc. At the low level control, by using robust-exact-differentiator-based (RED-based) ESOs for estimating the total disturbances in finite time, control Lyapunov functions (CLF) for assuring stability, and input-to-state safe high order control barrier functions (ISSf-HOCBF) for guaranteeing safety, constrained quadratic programs (QPs) are formulated to obtain optimal surge force and yaw moment. To facilitate real-time implementations, one-layer recurrent neural networks (RNNs) are employed to solve the constrained quadratic optimization problem on board. The tracking errors of the closed-loop system are proved to be uniformly ultimately bounded and the safety of the multi-ISV system is guaranteed. An application to the vessel train is given to substantiate the effectiveness of the proposed general safety-certified cooperative control architecture.

Compared with contributions in [7]–[9], [12]–[48], the main features of the proposed general safety-certified cooperative control architecture with control method are summarized into three-folds:

1) In contrast to the formation controllers in [7]–[9], [12]–[44] with specific coordinated control scenarios, this paper presents a general safety-certified cooperative control architecture consisting of a high-level distributed motion generator and a low-level tracking controller. The proposed cooperative control architecture is universal and takes the capabilities to be compatible with various coordinated control scenarios and achieve various collective behaviors.
2) In contrast to the collision avoidance strategies in [14]–[27], [45], [46], ISSf-HOCBFs are designed to construct the safety constraints from static/dynamic obstacles and neighboring vehicles. Within safety, stability, and input constraints, the optimal control force and moment are obtained in realtime by the designed RNNs without resorting to optimization tools.
3) In contrast to the disturbance observers in [16], [17], [26], [34], [47], the proposed RED-based ESOs can estimate the unknown total disturbances in finite time. Different from the fuzzy/NN approximation approaches in [14], [15], [20], [21], [24], [25], [28], [33], [35], [48], RED-based ESOs takes a simpler estimation structure and fewer tuning parameters.

This paper is organized as follows. Section II states preliminaries and problem formulation. Section III designs the controller. Section IV analyzes the stability and the safety of the closed-loop system. Section V gives simulation results. Section VI concludes this paper.

II. Preliminaries and Problem Formulation

A. Notation

For a vector $a = [a_1, \ldots, a_n]^T \in \mathbb{R}^n$ and a constant $b \in (0, 1)$, we define the symbol $\lceil a \rfloor^b = [\lceil a_1 \rfloor^b, \ldots, \lceil a_n \rfloor^b]^T$ with $\lceil a_i \rfloor^b = \mathrm{sgn}(a_i)|a_i|^b$, $i = 1, \ldots, n$, where $\mathrm{sgn}(\cdot)$ is a signum function. A continuous function $\kappa(\cdot) : (c, d) \mapsto \mathbb{R}$ is named as an extended class $\mathcal{K}$ function ($\kappa(\cdot) \in \mathcal{K}_e$) with $c, d > 0$, iff $\kappa(\cdot)$ is strictly monotonically increasing and $\kappa(0) = 0$. It is called as an extended class $\mathcal{K}_\infty$ function ($\kappa(\cdot) \in \mathcal{K}_{\infty,e}$) when $c, d \mapsto \infty$ and $\lim_{\iota \mapsto \infty} \kappa(\iota) = \infty$, $\lim_{\iota \mapsto -\infty} \kappa(\iota) = -\infty$. ess sup $(\cdot)$ denotes the essential supremum of $(\cdot)$.

B. Input-to-State Safe High Order Control Barrier Function

Consider an affine control system with disturbances $\omega \in \mathbb{R}^n$ in this form

$$\dot{x} = f(x) + g(x)u + \omega, \tag{1}$$

where $x \in \mathbb{R}^n$ is the system state. $u \in \mathbb{R}^m$ is the control input. $f(x) \in \mathbb{R}^n$ and $g(x) \in \mathbb{R}^{n \times m}$ are locally Lipschitz continuous functions. ω is assumed to be bounded and satisfied with $\|\omega\|_\infty \triangleq \mathrm{ess\,sup}_{t>0} \|\omega\|$.

Definition 1 ([49]): For a system (1) with $\omega = 0$, a super-level set $\mathcal{C} \subset \mathbb{R}^n$ with a continuously differentiable function $h(x) : \mathbb{R}^n \mapsto \mathbb{R}$ is defined as

$$\begin{aligned} \mathcal{C} &= \{x \in \mathbb{R}^n : h(x) \geq 0\}, \\ \partial\mathcal{C} &= \{x \in \mathbb{R}^n : h(x) = 0\}, \\ \mathrm{Int}(\mathcal{C}) &= \{x \in \mathbb{R}^n : h(x) > 0\}. \end{aligned} \tag{2}$$

Then, the set $\mathcal{C}$ is forward invariant if there is $x(t) \in \mathcal{C}$ for any $x(t_0) \in \mathcal{C}$, $\forall\, t \geq t_0$. The forward invariance of $\mathcal{C}$ indicates that the system (1) with $\omega = 0$ is safe on $\mathcal{C}$.

Definition 2 ([49]): For a system (1), an extended set $\mathcal{C}_\omega \supset \mathcal{C}$ with the continuous functions $h(x)$ is defined as follows

$$\begin{aligned} \mathcal{C}_\omega &= \{x \in \mathbb{R}^n : h(x) + \kappa_\omega(\|\omega\|_\infty) \geq 0\}, \\ \partial\mathcal{C}_\omega &= \{x \in \mathbb{R}^n : h(x) + \kappa_\omega(\|\omega\|_\infty) = 0\}, \\ \mathrm{Int}(\mathcal{C}_\omega) &= \{x \in \mathbb{R}^n : h(x) + \kappa_\omega(\|\omega\|_\infty) > 0\}. \end{aligned} \tag{3}$$

The set $\mathcal{C}_\omega$ is forward invariant for all $\|\omega\|_\infty \le \bar{\omega} \in \mathbb{R}^+$, if there exist a control input u and a function $\kappa_\omega(\cdot) \in \mathcal{K}_\infty$. Then, the system (1) is input-to-state safe (ISSf) on $\mathcal{C}$ as in (2) if the forward invariant set $\mathcal{C}_\omega$ is existed.

For a continuously differentiable function $h(x)$ with a relative degree $d > 1$, we define a series of functions $\chi_i : \mathbb{R}^n \mapsto \mathbb{R}$ and corresponding sets $\mathcal{C}_{i\omega}$ as follows

$$\begin{cases} \chi_i(x) = \dot{\chi}_{i-1}(x) + \kappa_i\left(\chi_{i-1}(x)\right), \\ \mathcal{C}_{i\omega} = \{x \in \mathbb{R}^n : \chi_{i-1}(x) \ge -\kappa_{i\omega}(\|\omega\|_\infty)\}, \end{cases} \tag{4}$$

where $\chi_0(x) = h(x)$, $i = 1, \ldots d$, and $\kappa_i(\cdot) \in \mathcal{K}_{\infty,e}$.

Definition 3 ([49]): Given functions $\chi_1(x), \ldots, \chi_d(x)$ and sets $\mathcal{C}_{1\omega}, \ldots, \mathcal{C}_{d\omega}$ defined by (4), the continuously differentiable function $h(x)$ with relative degree $d > 1$ is called as an ISSf-HOCBF for system (1) on the set $\mathcal{C}$, if there exist a constant $\bar{\omega} > 0$ and functions $\kappa_d(\cdot) \in \mathcal{K}_{\infty,e}$, $\kappa_{d\omega}(\cdot) \in \mathcal{K}_\infty$ such that for all $x \in \mathbb{R}^n$ and $\omega \in \mathbb{R}^n$ with $\|\omega\|_\infty \le \bar{\omega}$

$$\sup_{u \in \mathbb{R}^m}\left[L_f^d h(x) + L_g L_f^{d-1} h(x) u + \frac{\partial \chi_{d-1}(x)}{\partial x^T}\omega + \kappa_d\left(\chi_{d-1}(x)\right)\right] \ge -\kappa_{d\omega}(\|\omega\|_\infty), \tag{5}$$

where $L_f^d h$ and $L_g L_f^{d-1} h$ represent the Lie derivatives of $h(x)$.

Lemma 1 ([49]): Given an ISSf-HOCBF $h(x)$ defined by Def. 3 for system (1) on $\mathcal{C}$, any Lipschitz continuous controller $u \in \mathcal{U}(x)$ for all $x \in \mathbb{R}^n$ satisfying

$$\mathcal{U}(x) = \left\{u \in \mathbb{R}^m : L_f^d h(x) + L_g L_f^{d-1} h(x) u + \frac{\partial \chi_{d-1}(x)}{\partial x^T}\omega + \kappa_d\left(\chi_{d-1}(x)\right) \ge -\kappa_{d\omega}(\|\omega\|_\infty)\right\} \tag{6}$$

yields that the set $\mathcal{C}_{1\omega} \cap \mathcal{C}_{2\omega} \cap, \ldots, \cap \mathcal{C}_{d\omega}$ is forward invariant, which means that the system (1) is ISSf on $\mathcal{C}$.

Noting that the term ω may be unavailable for a practical system. Hereby, the following theorem is given.

Theorem 1: Given a series of functions $\chi_1(x), \ldots, \chi_d(x)$ and sets $\mathcal{C}_{1\omega}, \ldots, \mathcal{C}_{d\omega}$ defined by (4), the continuously differentiable function $h(x)$ of relative degree $d > 1$ is called as ISSf-HOCBF for the system (1) on the set $\mathcal{C}$, if there exist a constant $\bar{\omega} > 0$ and a function $\kappa_d(\cdot) \in \mathcal{K}_{\infty,e}$ such that for all $x \in \mathbb{R}^n$ and $\omega \in \mathbb{R}^n$ with $\|\omega\|_\infty \le \bar{\omega}$

$$\sup_{u \in \mathbb{R}^m}\left[L_f^d h(x) + L_g L_f^{d-1} h(x) u - \frac{\partial \chi_{d-1}(x)}{\partial x^T}\frac{\partial \chi_{d-1}(x)}{\partial x} + \kappa_d\left(\chi_{d-1}(x)\right)\right] \ge 0. \tag{7}$$

any Lipschitz continuous controller $u \in \mathcal{U}^*(x)$ satisfying

$$\mathcal{U}^*(x) = \left\{u \in \mathbb{R}^m : L_f^d h(x) + L_g L_f^{d-1} h(x) u - \frac{\partial \chi_{d-1}(x)}{\partial x^T}\frac{\partial \chi_{d-1}(x)}{\partial x} + \kappa_d\left(\chi_{d-1}(x)\right) \ge 0\right\}. \tag{8}$$

devises the system ISSf on the set $\mathcal{C}$.

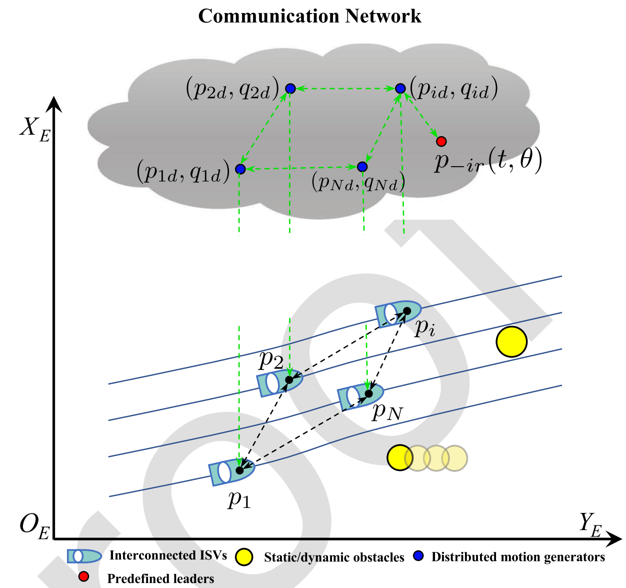

Fig. 1. Cooperative control scenario of ISVs subject to static/dynamic obstacles.

Proof: From (4), taking the derivative of $\chi_d(x)$ yields

$$\dot{\chi}_d = L_f^d h(x) + L_g L_f^{d-1} h(x) u + \frac{\partial \chi_{d-1}}{\partial x^T}\omega + \kappa_d(\chi_{d-1}). \tag{9}$$

For $u \in \mathcal{U}^*(x)$, one has

$$\dot{\chi}_d \ge \left(\left\|\frac{\partial \chi_{d-1}(x)}{\partial x}\right\| - \frac{\|\omega\|}{2}\right)^2 - \frac{\|\omega\|^2}{4} \ge -\frac{\|\omega\|^2}{4}. \tag{10}$$

Obviously, the inequality (10) is in the form of (5). It is concluded that the function $h(x)$ is ISSf-HOCBF of system (1) and the set $\mathcal{U}^*(x)$ satisfies $\mathcal{U}^*(x) \subseteq \mathcal{U}(x)$. It means that Theorem 1 holds. The proof is completed.

C. Problem Formulation

Consider a networked system with N underactuated ISVs shown in Fig. 1. It is assumed that each ISV has a plane of symmetry; heave, pitch, and roll modes are neglected. The kinematic and kinetic dynamics of the ith ISV are described as follows [26]

$$\begin{cases} \dot{\eta}_i = R_i(\psi_i)\nu_i, \\ M_i \dot{\nu}_i = f_i(\nu_i) + \tau_i + \tau_{iw}, \end{cases} \tag{11}$$

where $i = 1, \ldots, N$. $\eta_i = [p_i^T, \psi_i]^T$ denotes the position and yaw angular with $p_i = [x_i, y_i]^T \in \mathbb{R}^2$ and $\psi_i \in (-\pi, \pi]$. $\nu_i = [u_i, v_i, r_i]^T \in \mathbb{R}^3$ represents the body-fixed velocity vector along the surge, sway and yaw direction. $M_i = \text{diag}\{m_i^u, m_i^v, m_i^r\} \in \mathbb{R}^3$ is the inertia mass matrix. $f_i(\nu_i) \in \mathbb{R}^3$ is the unknown function including Coriolis terms, damping terms and unmodeled dynamics. $\tau_i = [\tau_i^u, 0, \tau_i^r]^T$ is a bounded control input satisfying $0 \le \tau_i^u \le \bar{\tau}_i^u$ and $-\bar{\tau}_i^r \le \tau_i^r \le \bar{\tau}_i^r$ with $\bar{\tau}_i^u \in \mathbb{R}^+$ and $\bar{\tau}_i^r \in \mathbb{R}^+$ being bounds of input signals. $\tau_{iw} \in \mathbb{R}^3$ presents the unknown environmental disturbances due to wind, wave and current. $R_i(\psi_i) = \text{diag}\{R_i^p(\psi_i), 1\}$ is a rotation matrix with $R_i^p(\psi_i) = [\cos(\psi_i), -\sin(\psi_i); \sin(\psi_i), \cos(\psi_i)]$.

To design the safety-certified controllers, the model dynamics (11) is rewritten as

$$\begin{cases} \dot{p}_i = q_i, & (12a)\\ \dot{q}_i = \sigma_i^q + \tau_i^q/m_i^u, & (12b)\\ \dot{\psi}_i = r_i, & (12c)\\ \dot{r}_i = \sigma_i^r + \tau_i^r/m_i^r, & (12d)\end{cases}$$

where $q_i = R_i^p(\psi_i)[u_i, v_i]^T$ and $[\sigma_i^{qT}, \sigma_i^r]^T = \dot{R}_i(\psi_i)\nu_i + R_i(\psi_i)M_i^{-1}(f_i(\nu_i) + \tau_{iw})$ with $\sigma_i^q = [\sigma_i^x, \sigma_i^y]^T \in \mathbb{R}^2$ and $\sigma_i^r \in \mathbb{R}$ being unknown earth-fixed disturbances. $\tau_i^q = [\tau_i^x, \tau_i^y]^T \in \mathbb{R}^2$ stands for the earth-fixed control input satisfying $\tau_i^x = \tau_i^u \cos(\psi_i)$ and $\tau_i^y = \tau_i^u \sin(\psi_i)$.

This paper aims to present a general safety-certified cooperative control architecture for underactuated ISVs subject to static/dynamic obstacles to achieve the following objectives:

1) *Geometric Objective:* Force each ISV to track the reference trajectory $p_{id} = [x_{id}, y_{id}]^T$ such that

$$\|p_i - p_{id}\| < \mu, \tag{13}$$

where $i = 1, \ldots, N$ and $\mu \in \mathbb{R}^+$.

2) *Safety Objective:* To guarantee the safety of multi-ISV system, the following distance constraints are required to be satisfied:

1) Inter-ISV collision avoidance:

$$\|p_i - p_j\| > R_c, \tag{14}$$

where $i, j = 1, \ldots, N, i \neq j$. $R_c \in \mathbb{R}^+$ is the minimum collision-free distance among neighboring ISVs.

2) Obstacle collision avoidance:

$$\|p_i - p_o\| > R_o + \rho_o, \tag{15}$$

where $i = 1, \ldots, N$, $o = 1, \ldots, N_o$ with $N_o \in \mathbb{R}^+$ being the total number of obstacles. $p_o \in \mathbb{R}^2$ presents the position of obstacle. $R_o \in \mathbb{R}^+$ is the minimum collision-free distance from obstacles. $\rho_o \in \mathbb{R}^+$ is the radius of the oth obstacle.

III. General Cooperative Control Architecture

A. High Level Distributed Motion Generator

Based on the vehicle model in (11), a series of distributed cooperative control schemes are presented to achieve various collective behaviors such as consensus [16], containment [18], flocking [17], and enclosing [28]. In [16], [18], [28], the control laws are designed for specific formations. Once the mission is changed, the control law has to be switched. To remedy this limitation, a general safety-certified cooperative control architecture for multiple ISVs is proposed, which are able to achieve various formation without modifying the low-level control laws. As shown in Fig. 2, it includes a high-level motion generator and a low-level trajectory tracking controller. Motivated by the distributed cooperative control laws in for achieving consensus, containment, enclosing, and flocking, a distributed motion generator is proposed as follows

$$\begin{cases} \dot{p}_{id} = q_{id},\\ \dot{q}_{id} = \hbar_i(p_{-ir}(t,\theta), p_{id}, q_{id}, p_{-id}, q_{-id}), \end{cases} \tag{16}$$

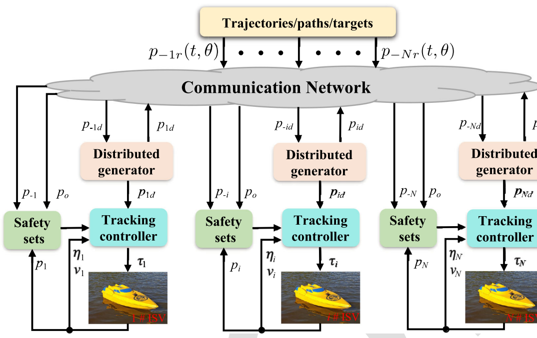

Fig. 2. A general safety-certified cooperative control architecture for ISVs.

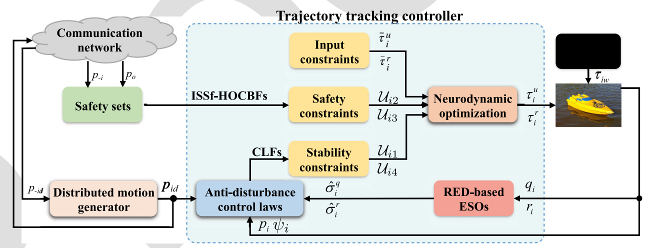

Fig. 3. The low-level safety-certified control architecture.

where $p_{id} \in \mathbb{R}^2$ and $q_{id} \in \mathbb{R}^2$ are the states of the generator. $p_{-ir}(t,\theta) = \{p_{lr}(t,\theta_l)\}_{l\in\mathcal{N}_i^L}$ is the predefined input signal, which may be the trajectory, the path or the target with $\theta_l \in \mathbb{R}$ being a path parameter. p_{-id} and q_{-id} are output signals of the ith generator's neighbors satisfying $p_{-id} = \{p_{kd}\}_{k\in\mathcal{N}_i^F}$ and $q_{-id} = \{q_{kd}\}_{k\in\mathcal{N}_i^F}$. $\hbar_i(\cdot) \in \mathbb{R}^2$ are known, bounded and Lipschitz functions, which can be designed by the specific mission scenarios.

B. Low Level Trajectory Tracking Controller

In this subsection, a safety-certified cooperative control law is developed for ISVs to track the reference trajectory. Fig. 3 presents the block diagram of the proposed low-level controller for the ith ISV.

1) The Optimal Surge Force Controller: The ESO is an effective and appealing tool to address the unknow uncertainties [50]. To estimate the unknown term σ_i^q in (12b), the RED-based ESO is proposed as follows

$$\begin{cases} \dot{\hat{q}}_i = -k_{i1}^q \zeta_i^{q\frac{1}{2}} \lceil \hat{q}_i - q_i \rfloor^{\frac{1}{2}} + \hat{\sigma}_i^q + \tau_i^q/m_i^u,\\ \dot{\hat{\sigma}}_i^q = -k_{i2}^q \zeta_i^q \mathrm{sgn}(\hat{q}_i - q_i), \end{cases} \tag{17}$$

where $\hat{q}_i = [\hat{q}_i^x, \hat{q}_i^y]^T \in \mathbb{R}^2$ and $\hat{\sigma}_i^q = [\hat{\sigma}_i^x, \hat{\sigma}_i^y]^T \in \mathbb{R}^2$ represent the estimated values of q_i and σ_i^q, respectively. k_{i1}^q and k_{i2}^q are positive constants. $\zeta_i^q \in \mathbb{R}^+$ is a scaling factor.

Define the estimated errors $\tilde{q}_i = (\hat{q}_i - q_i)/\zeta_i^q$ and $\tilde{\sigma}_i^q = (\hat{\sigma}_i^q - \sigma_i^q)/\zeta_i^q$. Combining (12a)-(12b) with (17), the time derivatives of $\tilde{q}_i$ and $\tilde{\sigma}_i^q$ are deduced as follows

$$\begin{cases} \dot{\tilde{q}}_i = -k_{i1}^q \lceil \tilde{q}_i \rfloor^{\frac{1}{2}} + \tilde{\sigma}_i^q,\\ \dot{\tilde{\sigma}}_i^q = -k_{i2}^q \mathrm{sgn}(\tilde{q}_i) - \dot{\sigma}_i^q/\zeta_i^q. \end{cases} \tag{18}$$

Letting $z_{i1} = p_i - p_{id}$ and taking its derivative with (12a), (12b), and (16), it yields that

$$\dot{z}_{i1} = q_i - q_{id} \text{ and } \ddot{z}_{i1} = \sigma_i^q + \tau_i^q / m_i^u - \dot{q}_{id}. \tag{19}$$

To stabilize the error dynamics $\ddot{z}_{i1}$, by using the estimated information from RED-based ESO, an anti-disturbance control law is presented as follows

$$\tau_i^q = m_i^u(\dot{q}_{id} + \tau_i^{q*} - \hat{\sigma}_i^q) \tag{20}$$

with $\tau_i^{q*} = [\tau_i^{x*}, \tau_i^{y*}]^T$ being an earth-fixed optimal control signals. Substituting (20) into (19), one has

$$\dot{z}_{i1} = q_i - q_{id} \text{ and } \ddot{z}_{i1} = -\tilde{\sigma}_i^q + \tau_i^{q*}. \tag{21}$$

To obtain optimal surge force τ_i^u, the following constraints are constructed to achieve stability and safety.

Step 1. CLF-based stability constraint

Let $Z_{i1} = [z_{i1}^T, \dot{z}_{i1}^T]^T$ and take its derivative along (21) as

$$\dot{Z}_{i1} = A_{i1} Z_{i1} + B_{i1}(-\tilde{\sigma}_i^q + \tau_i^{q*}) \tag{22}$$

with $A_{i1} = [0_2, I_2; 0_2, 0_2]$ and $B_{i1} = [0_2, I_2]^T$.

To stabilize Z_{i1}, a candidate Lyapunov function V_{i1} is constructed as follows

$$V_{i1} = Z_{i1}^T P_{i1} Z_{i1}, \tag{23}$$

where $P_{i1} = P_{i1}^T$ is a positive-definite matrix such that the continuous algebraic Riccati equation

$$A_{i1}^T P_{i1} + P_{i1} A_{i1} - \frac{P_{i1} B_{i1} B_{i1}^T P_{i1} - D_{i1} Q_{i1} D_{i1}}{\gamma_{i1}} = 0, \tag{24}$$

where γ_{i1} is a positive constant. Q_{i1} represents a symmetric positive-definite matrix and $D_{i1} = [I_2/\gamma_{i1}, 0_2; 0_2, I_2]$.

Apply the transform $P_{i1} = D_{i1} P_{i1}' D_{i1}$, where $P_{i1}' = P_{i1}'^T > 0$ satisfies

$$A_{i1}^T P_{i1}' + P_{i1}' A_{i1} - P_{i1}' B_{i1} B_{i1}^T P_{i1}' + Q_{i1} = 0. \tag{25}$$

Based on the dynamics (22), a CLF-based stability constraint set for the optimal signal τ_i^{q*} is constructed as [51]

$$\mathcal{U}_{i1} = \left\{ \tau_i^{q*} : L_{A_{i1}} V_{i1} + L_{B_{i1}} V_{i1} \tau_i^{q*} + \frac{\epsilon_{i1}}{\gamma_{i1}} V_{i1} \le 0 \right\}, \tag{26}$$

where $L_{A_{i1}} V_{i1} = Z_{i1}^T (P_{i1} A_{i1} + A_{i1}^T P_{i1}) Z_{i1}$, $L_{B_{i1}} V_{i1} = 2 Z_{i1}^T P_{i1} B_{i1}$ and $\epsilon_{i1} = \lambda_{\min}(Q_{i1}) / \bar{\lambda}(P_{i1}')$.

To calculate the open-loop solution in (26), a position pointwise min-norm control law is developed as follows

$$\tau_i^{q*} = \begin{cases} -\Psi_{i1}\Psi_{i2}/(\Psi_{i2}^T \Psi_{i2}), & \text{if } \Psi_{i1} > 0, \\ 0, & \text{if } \Psi_{i1} \le 0, \end{cases} \tag{27}$$

where $\Psi_{i1} = L_{A_{i1}} V_{i1} + \epsilon_{i1} V_{i1} / \gamma_{i1} + \varrho_{i1} \| L_{B_{i1}} V_{i1} \|$ and $\Psi_{i2} = L_{B_{i1}} V_{i1}$ with ϱ_{i1} being a positive constant.

Step 2. ISSf-HOCBF-based safety constraints

Substituting (20) into (12b), the dynamic subsystem (12a)-(12b) can be rewritten as follows

$$\dot{e}_i = f_i + g_i \tau_i^{q*} + \omega_i, \tag{28}$$

where $e_i = [p_i^T, q_i^T]^T$, $f_i = [q_i^T, 0_2]^T$, $g_i = [0_2, I_2]^T$ and $\omega_i = [0_2, \dot{q}_{id}^T - \tilde{\sigma}_i^{qT}]^T$.

From Def. 1, safety objectives (14) and (15) are encoded into super-level sets $\mathcal{C}_{ij}$ and $\mathcal{C}_{io}$, respectively. It means that the forward invariance of sets $\mathcal{C}_{ij}$ and $\mathcal{C}_{io}$ are equivalent to the safety of the ith ISV. Then, we aim to devise the control constraint sets for ensuring forward invariance of $\mathcal{C}_{ij}$ and $\mathcal{C}_{io}$.

In order to avoid collision among ISVs, the set $\mathcal{C}_{ij}$ is constructed as follows

$$\mathcal{C}_{ij} = \left\{ p_i \in \mathbb{R}^2 : h_{ij}(p_i) = \|p_{ij}\|^2 - R_c^2 \ge 0 \right\}, \tag{29}$$

where $p_{ij} = p_i - p_j$. $h_{ij}(p_i)$ is a candidate ISSf-HOCBF.

From (4), a family of functions with $h_{ij}(p_i)$ are defined as $\chi_{ij,0} = h_{ij}, \chi_{ij,1} = \dot{\chi}_{ij,0} + \kappa_{i1}(\chi_{ij,0}), \chi_{ij,2} = \dot{\chi}_{ij,1} + \kappa_{i2}(\chi_{ij,1})$, and the corresponding safety sets are denoted as $\mathcal{C}_{ij,1} = \{p_i \in \mathbb{R}^2 : \chi_{ij,0} \ge \kappa_{i\omega,1}(\|\omega_i\|_\infty)\}$ and $\mathcal{C}_{ij,2} = \{p_i \in \mathbb{R}^2 : \chi_{ij,1} \ge \kappa_{i\omega,2}(\|\omega_i\|_\infty)\}$, where $\kappa_{i1}(\cdot)$, $\kappa_{i2}(\cdot) \in \mathcal{K}$ and $\kappa_{i\omega,1}(\cdot), \kappa_{i\omega,2}(\cdot) \in \mathcal{K}_\infty$.

According to (6) and (28), the safety constraint of the control input for the ith ISV is devised as

$$\mathcal{U}_{i2} = \left\{ \tau_i^{q*} : L_{f_i}^2 h_{ij} + L_{g_i} L_{f_i} h_{ij} \tau_i^{q*} - \frac{\partial \chi_{ij,1}(p_i)}{\partial p_i^T} \frac{\partial \chi_{ij,1}(p_i)}{\partial p_i} + \kappa_{i2}(\chi_{ij,1}) \ge 0 \right\}, \tag{30}$$

where $L_{f_i}^2 h_{ij} = 2(q_i - q_j)^T (q_i - q_j)$ and $L_{g_i} L_{f_i} h_{ij} = 2 p_{ij}^T$.

To avoid collision between ISVs and static/dynamic obstacles, the safe set $\mathcal{C}_{io}$ is developed as follows

$$\mathcal{C}_{io} = \{p_i \in \mathbb{R}^2 : h_{io}(p_i) = \|p_{io}\|^2 - (R_o + \rho_o)^2 \ge 0\} \tag{31}$$

where $p_{io} = p_i - p_o$.

Similarly, the safety constraint with $h_{io}(p_i)$ is described as

$$\mathcal{U}_{i3} = \left\{ \tau_i^{q*} : L_{f_i}^2 h_{io} + L_{g_i} L_{f_i} h_{io} \tau_i^{q*} - \frac{\partial \chi_{ij,1}(p_i)}{\partial p_i^T} \frac{\partial \chi_{ij,1}(p_i)}{\partial p_i} + \kappa_{i2}(\chi_{io}) \ge 0 \right\}, \tag{32}$$

where $L_{f_i}^2 h_{io} = 2(q_i - q_o)^T (q_i - q_o)$, $L_{g_i} L_{f_i} h_{io} = 2 p_{io}^T$, and $\chi_{io} = \dot{h}_{io} + \kappa_{i1}(h_{io})$.

Step 3. QP-based optimal surge force

For the cooperative formation of multiple ISVs, the safety objective has higher priority than the geometric objective. To unify the designed stability constraint (26), safety constraints (30), (32) and input constraints, a quadratic optimization problem is formulated as follows

$$\begin{aligned} \tau_i^{q*} = \underset{[\tau_i^{q*}; \delta_i] \in \mathbb{R}^3}{\operatorname{argmin}} \quad & J_i^q(\tau_i^{q*}) = \|\tau_i^{q*}\|^2 + l_i \delta_i^2 \\ \text{s.t.} \quad & \Psi_{i2}(Z_{i1}) \tau_i^{q*} \le b_{i1}, \\ & -L_{g_i} L_{f_i} h_{ij} \tau_i^{q*} \le b_{i2}, \\ & -L_{g_i} L_{f_i} h_{io} \tau_i^{q*} \le b_{i3}, \\ & \underline{\tau}_i^{q*} \le \tau_i^{q*} \le \bar{\tau}_i^{q*}, \end{aligned} \tag{33}$$

where δ_i is a relaxation variable. $l_i \in \mathbb{R}^+$ denotes a penalty coefficient. $b_{i1} = -\Psi_{i1}(Z_{i1}) + \delta_i$, $b_{i2} = L_{f_i}^2 h_{ij} - (\partial \chi_{ij,1}(p_i)/\partial p_i^T)(\partial \chi_{ij,1}(p_i)/\partial p_i) + \kappa_{i2}(\chi_{ij,1})$, $b_{i3} = L_{f_i}^2 h_{io} - (\partial \chi_{ij,1}(p_i)/\partial p_i^T)(\partial \chi_{ij,1}(p_i)/\partial p_i) + \kappa_{i2}(\chi_{io})$, $\bar{\tau}_i^{q*} = \bar{\tau}_i^q / m_i^u + \hat{\sigma}_i^q - \ddot{p}_{id}$ and $\underline{\tau}_i^{q*} = -\bar{\tau}_i^q / m_i^u + \hat{\sigma}_i^q - \ddot{p}_{id}$.

A lot of optimization tools are capable of solving the constrained quadratic optimization problem in (33). However, most of the optimization methods may not be competent for real-time implementation. Thus, a one-layer RNN is employed to solve the optimization problem in (33) as follows [52]

$$\varepsilon_i^q \dot{\tau}_i^{q*} = -\nabla J_i^q(\tau_i^{q*}) - \frac{1}{\iota_i^q}\partial \sum_{k=1}^{N+N_o+2} \max\{0, \xi_{ik}^q\} \tag{34}$$

where $\varepsilon_i^q \in \mathbb{R}^+$ is a time constant. ι_i^q is a penalty parameter. $\xi_{i1}^q = \Psi_{i2}(Z_{i1})\tau_i^{q*} - b_{i1}$, $\xi_{ik}^q = -L_{g_i}L_{f_i}h_{ij}\tau_i^{q*} - b_{i2}$, $k = 2,\ldots,N$, $\xi_{ik}^q = -L_{g_i}L_{f_i}h_{io}\tau_i^{q*} - b_{i3}$, $k = N+1,\ldots,N+N_o$, $\xi^q_{i(N+N_o+1)} = \tau_i^{q*} - \bar{\tau}_i^{q*}$ and $\xi^q_{i(N+N_o+2)} = -\tau_i^{q*} + \underline{\tau}_i^{q*}$. $\partial \max\{0, \xi_{ik}^q\}$ is an exact penalty function expressed as

$$\partial \max\{0, \xi_{ik}^q\} = \begin{cases} \nabla \xi_{ik}^q, & \text{for } \xi_{ik}^q > 0, \\ [0,1]\nabla \xi_{ik}^q, & \text{for } \xi_{ik}^q = 0, \\ 0_2, & \text{for } \xi_{ik}^q < 0 \end{cases}$$

with [0, 1] is a set-valued map with image in the scope [0, 1]. By the literature [52], the neuronal state τ_i^{q*} of above RNN is exponentially convergent to the optimal solution in finite time.

Since $\tau_i^x = \tau_i^u \cos(\psi_i)$ and $\tau_i^y = \tau_i^u \sin(\psi_i)$, the optimal surge force τ_i^u and the desired yaw angle ψ_{ir} are given as

$$\begin{cases} \tau_i^u = \tau_i^x \cos(\psi_i) + \tau_i^y \sin(\psi_i), \\ \psi_{ir} = \text{atan2}\left(\tau_i^y, \tau_i^x\right), \end{cases} \tag{35}$$

where atan2$(\cdot)$ is a four quadrant inverse tangent function.

2) The Optimal Yaw Moment Controller: To obtain the time derivatives of ψ_{ir}, an RED-based nonlinear tracking differentiator (RED-basde NLTD) is presented as follows

$$\begin{cases} \dot{\Theta}_{i1} = -k_{i1}^{\Theta}\zeta_i^{\Theta\frac{1}{3}}\lceil \Theta_{i1} - \psi_{ir}\rfloor^{\frac{2}{3}} + \Theta_{i2}, \\ \dot{\Theta}_{i2} = -k_{i2}^{\Theta}\zeta_i^{\Theta\frac{2}{3}}\lceil \Theta_{i1} - \psi_{ir}\rfloor^{\frac{1}{3}} + \Theta_{i3}, \\ \dot{\Theta}_{i3} = -k_{i3}^{\Theta}\zeta_i^{\Theta}\text{sgn}(\Theta_{i1} - \psi_{ir}), \end{cases} \tag{36}$$

where Θ_{i1}, Θ_{i2} and Θ_{i3} represent the estimations of ψ_{ir}, $\dot{\psi}_{ir}$ and $\ddot{\psi}_{ir}$, respectively. k_{i1}^{Θ}, k_{i2}^{Θ} and k_{i3}^{Θ} are the positive designed constants. $\zeta_i^{\Theta} \in \mathbb{R}^+$ is a scaling factor.

Define the estimated errors $\tilde{\Theta}_{i1} = \Theta_{i1} - \psi_{ir}$, $\tilde{\Theta}_{i2} = \Theta_{i2} - \dot{\psi}_{ir}$ and $\tilde{\Theta}_{i3} = \Theta_{i3} - \ddot{\psi}_{ir}$. The time derivatives of $\tilde{\Theta}_{i1}$, $\tilde{\Theta}_{i2}$ and $\tilde{\Theta}_{i3}$ are inferred as follows

$$\begin{cases} \dot{\tilde{\Theta}}_{i1} = -k_{i1}^{\Theta}\zeta_i^{\Theta\frac{1}{3}}\lceil \tilde{\Theta}_{i1}\rfloor^{\frac{2}{3}} + \tilde{\Theta}_{i2}, \\ \dot{\tilde{\Theta}}_{i2} = -k_{i2}^{\Theta}\zeta_i^{\Theta\frac{2}{3}}\lceil \tilde{\Theta}_{i1}\rfloor^{\frac{1}{3}} + \tilde{\Theta}_{i3}, \\ \dot{\tilde{\Theta}}_{i3} = -k_{i3}^{\Theta}\zeta_i^{\Theta}\text{sgn}(\tilde{\Theta}_{i1}) - \psi_{ir}^{(3)}, \end{cases} \tag{37}$$

where $\psi_{ir}^{(3)}$ represents the time derivative of $\ddot{\psi}_{ir}$ satisfying $|\psi_{ir}^{(3)}| \leq \bar{\psi}_{ir} \in \mathbb{R}^+$. According to Theorem 4 in [53], the error dynamics (37) are finite-time stable. Thus, it is also means that the estimation errors $\tilde{\Theta}_{i1}$, $\tilde{\Theta}_{i2}$ and $\tilde{\Theta}_{i3}$ are bounded and satisfied with $\|[\tilde{\Theta}_{i1}, \tilde{\Theta}_{i2}, \tilde{\Theta}_{i3}]\| \leq \bar{\Theta}_i \in \mathbb{R}^+$.

To recover the unknown disturbance σ_i^r, an RED-based ESO is proposed as follows

$$\begin{cases} \dot{\hat{r}}_i = -k_{i1}^r\zeta_i^{r\frac{1}{2}}\lceil \hat{r}_i - r_i\rfloor^{\frac{1}{2}} + \hat{\sigma}_i^r + \tau_i^r/m_i^r, \\ \dot{\hat{\sigma}}_i^r = -k_{i2}^r\zeta_i^r\text{sgn}(\hat{r}_i - r_i), \end{cases} \tag{38}$$

where $\hat{r}_i$ and $\hat{\sigma}_i^r$ present the estimated values of r_i and σ_i^r, respectively. k_{i1}^r, $k_{i2}^r \in \mathbb{R}^+$ are the predefined observer gains. $\zeta_i^r \in \mathbb{R}^+$ is a scaling factor.

Letting $\tilde{r}_i = (\hat{r}_i - r_i)/\zeta_i^r$ and $\tilde{\sigma}_i^r = (\hat{\sigma}_i^r - \sigma_i^r)/\zeta_i^r$ the time derivatives of $\tilde{r}_i$ and $\tilde{\sigma}_i^r$ are presented as follows

$$\begin{cases} \dot{\tilde{r}}_i = -k_{i1}^r\lceil \tilde{r}_i\rfloor^{\frac{1}{2}} + \tilde{\sigma}_i^r, \\ \dot{\tilde{\sigma}}_i^r = -k_{i2}^r\text{sgn}(\tilde{r}_i) - \dot{\sigma}_i^r/\zeta_i^r. \end{cases} \tag{39}$$

Define a yaw tracking error $z_{i2} = \psi_i - \psi_{ir}$. The dynamic of z_{i2} along (12c)-(12d) and (35) can be deduced as follows

$$\dot{z}_{i2} = r_i - \dot{\psi}_{ir} \text{ and } \ddot{z}_{i2} = \sigma_i^r + \tau_i^r/m_i^r - \ddot{\psi}_{ir}. \tag{40}$$

To stabilize the error dynamic $\ddot{z}_{i2}$, a yaw control law is developed as follows

$$\tau_i^r = m_i^r\left(\ddot{\psi}_{ir} + \tau_i^{r*} - \hat{\sigma}_i^r\right), \tag{41}$$

where τ_i^{r*} is a optimal yaw moment.

Substituting (41) into (40), it has

$$\dot{z}_{i2} = r_i - \dot{\psi}_{ir} \text{ and } \ddot{z}_{i2} = -\tilde{\sigma}_i^r + \tau_i^{r*}. \tag{42}$$

To solve the optimal yaw moment τ_i^r, the following constraints are constructed to achieve the yaw stability.

Step 1. CLF-based stability constraint

To simplify the constraint design, the error dynamics (40) can be transformed as follows

$$\dot{Z}_{i2} = A_{i2}Z_{i2} + B_{i2}(-\tilde{\sigma}_i^r + \tau_i^{r*}), \tag{43}$$

where $Z_{i2} = [z_{i2}, \dot{z}_{i2}]^T$, $A_{i2} = [0,1;0,0]$ and $B_{i2} = [0,1]^T$.

To stabilize Z_{i2}, a Lyapunov function is developed as

$$V_{i2} = Z_{i2}^T P_{i2} Z_{i2}, \tag{44}$$

where P_{i2} is a positive definite matrix satisfying

$$A_{i2}^T P_{i2} + P_{i2}A_{i2} - \frac{P_{i2}B_{i2}B_{i2}^T P_{i2} - D_{i2}Q_{i2}D_{i2}}{\gamma_{i2}} = 0 \tag{45}$$

with $\gamma_{i2} \in \mathbb{R}^+$, $D_{i2} = \text{diag}\{1/\gamma_{i2}, 1\}$ and $Q_{i2} = Q_{i2}^T > 0$. $P_{i2} = D_{i2}P'_{i2}D_{i2}$ with $P'_{i2} = P_{i2}^{'T} > 0$ satisfying

$$A_{i2}^T P'_{i2} + P'_{i2}A_{i2} - P'_{i2}B_{i2}B_{i2}^T P'_{i2} + Q_{i2} = 0.$$

According to [51], the optimal yaw moment τ_i^{r*} should meet the following constraint:

$$\mathcal{U}_{i4} = \left\{\tau_i^{r*} : L_{A_{i2}}V_{i2} + L_{B_{i2}}V_{i2}\tau_i^{r*} + \frac{\epsilon_{i2}}{\gamma_{i2}}V_{i2} \leq 0\right\}, \tag{46}$$

where $L_{A_{i2}}V_{i2} = Z_{i2}^T(P_{i2}A_{i2} + A_{i2}^T P_{i2})Z_{i2}$, $L_{B_{i2}}V_{i2} = 2Z_{i2}^T P_{i2}B_{i2}$ and $\epsilon_{i2} = \lambda_{\min}(Q_{i2})/\bar{\lambda}(P'_{i2})$.

To acquire the open-loop solution in $\mathcal{U}_{i4}$, a yaw pointwise min-norm control law is designed as follows

$$\tau_i^{r*} = \begin{cases} -\Psi_{i3}\Psi_{i4}/(\Psi_{i4}^T\Psi_{i4}), & \text{if } \Psi_{i3} > 0, \\ 0, & \text{if } \Psi_{i3} \leq 0 \end{cases} \tag{47}$$

with $\Psi_{i3} = L_{A_{i2}}V_{i2} + \epsilon_{i2}V_{i2}/\gamma_{i2} + \varrho_{i2}\|L_{B_{i2}}V_{i2}\|$ and $\Psi_{i4} = L_{B_{i2}}V_{i2}$, where ϱ_{i2} is a positive constant.

Step 2. QP-based optimal yaw moment

To unify the yaw stability constraint (46) and input constraint, the optimal control input τ_i^{r*} is solved via the following quadratic optimization

$$\begin{aligned} \tau_i^{r*} = & \operatorname*{argmin}_{\tau_i^{r*}\in\mathbb{R}} J_i^r(\tau_i^{r*}) = (\tau_i^{r*})^2 \\ \text{s.t.} \quad & \Psi_{i4}(Z_{i2})\tau_i^{r*} \le -\Psi_{i3}(Z_{i2}), \\ & \underline{\tau}_i^{r*} \le \tau_i^{r*} \le \bar{\tau}_i^{r*}, \end{aligned} \tag{48}$$

where $\bar{\tau}_i^{r*} = \bar{\tau}_i^r/m_i^r - \ddot{\psi}_{ir} + \hat{\sigma}_i^r$ and $\underline{\tau}_i^{r*} = -\bar{\tau}_i^r/m_i^r - \ddot{\psi}_{ir} + \hat{\sigma}_i^r$.

In order to facilitate real-time implementation, a one-layer RNN is used to solve the QP problem as follows [52]

$$\varepsilon_i^r \dot{\tau}_i^{r*} = -\nabla J_i^r(\tau_i^{r*}) - \frac{1}{\iota_i^r}\partial \sum_{k=1}^{3} \max\{0, \xi_{ik}^r\} \tag{49}$$

where $\varepsilon_i^r \in \mathbb{R}^+$ is a time constant determining the convergence speed. ι_i^r is a penalty parameter. $\xi_{i1}^r = \Psi_{i4}(Z_{i2})\tau_i^{r*} + \Psi_{i3}(Z_{i2})$, $\xi_{i2}^r = \tau_i^{r*} - \bar{\tau}_i^{r*}$, $\xi_{i3}^r = -\tau_i^{r*} + \underline{\tau}_i^{r*}$. The function $\partial \max\{0, \xi_{ik}^r\}$ is an exact penalty function expressed as

$$\partial \max\{0, \xi_{ik}^r\} = \begin{cases} \nabla \xi_{ik}^r, & \text{for } \xi_{ik}^r > 0, \\ [0,1]\nabla \xi_{ik}^r, & \text{for } \xi_{ik}^r = 0, \\ 0_2, & \text{for } \xi_{ik}^r < 0. \end{cases}$$

It is proven in [52] that the state τ_i^{r*} of the RNN (49) can exponentially converge to the optimal solution in a finite time.

IV. Stability and Safety Analysis

This section analyzes the stability of the closed-loop system and the safety of the multi-ISV system.

A. Stability Analysis

To analyze the stability of RED-based ESO subsystems (18) and (39), the following assumption is needed.

Assumption 1: The time derivatives of σ_i^q and σ_i^r are bounded and satisfying $\|\dot{\sigma}_i^q\| \le \bar{\sigma}_i^q$ and $|\dot{\sigma}_i^r| \le \bar{\sigma}_i^r$ with $\bar{\sigma}_i^q, \bar{\sigma}_i^r$ being positive constants, respectively.

Letting $s_i^q = \operatorname{diag}\{|\tilde{q}_i^x|^{\frac12}, |\tilde{q}_i^y|^{\frac12}\}$ and $\varpi_i^q = -s_i^q \dot{\sigma}_i^q/\zeta_i^q$, it gets $\|\varpi_i^q\| \le \bar{\sigma}_i^q \|s_i^q\|/\zeta_i^q$ and $\tilde{\varpi}_i^q = \bar{\sigma}_i^{q2}\|s_i^q\|^2/\zeta_i^{q2} - \|\varpi_i^q\|^2$. Define $Z_{i3} = [\lceil \tilde{q}_i \rfloor^{\frac12}; \tilde{\sigma}_i^q]$, $S_i^q = \operatorname{diag}\{|\tilde{q}_i^x|^{\frac12}, |\tilde{q}_i^y|^{\frac12}, |\tilde{q}_i^x|^{\frac12}, |\tilde{q}_i^y|^{\frac12}\}$. Then, the error dynamics (18) can be rewritten as follows

$$\dot{Z}_{i3} = (S_i^q)^{-1}(A_{i3}Z_{i3} + B_{i3}\varpi_i^q), \tag{50}$$

where $A_{i3} = [-\frac12 k_{i1}^q I_2, \frac12 I_2; -k_{i2}^q I_2, 0_2]$ and $B_{i3} = [0_2; I_2]$.

Then, the stability of the RED-based ESO subsystem (17) is given via the following lemma.

Lemma 2: Under Assumption 1, the error dynamics of the RED-based ESO (17) can converge to the neighborhood the origin in finite time, if there exists symmetric positive definite matrices P_{i3} and Q_{i3} such that

$$A_{i3}^T P_{i3} + P_{i3}A_{i3} + P_{i3}B_{i3}B_{i3}^T P_{i3} + C_{i1}^T C_{i1} = -Q_{i3} \tag{51}$$

with $C_{i1} = \bar{\sigma}_i^q [I_2, 0_2]$.

Proof: Consider a Lyapunov function candidate V_1 as $V_1 = Z_{i3}^T P_{i3} Z_{i3}$ Along (50), taking the time derivative of V_1 yields $\dot{V}_1 = Z_{i3}^T(A_{i3}^T(S_i^q)^{-1}P_{i3} + P_{i3}(S_i^q)^{-1}A_{i3})Z_{i3} + Z_{i3}^T P_{i3}(S_i^q)^{-1}B_{i3}\varpi_i^q + \varpi_i^{qT} B_{i3}^T(S_i^q)^{-1}P_{i3}Z_{i3} \le \underline{\lambda}(S_i^q)(Z_{i3}^T (A_{i3}^T P_{i3} + P_{i3}A_{i3})Z_{i3} + Z_{i3}^T P_{i3}B_{i3}\varpi_i^q + \varpi_i^{qT} B_{i3}^T P_{i3} Z_{i3} + \|\tilde{\varpi}_i^q\|)$. From (51), $\dot{V}_1$ becomes $\dot{V}_1 \le \underline{\lambda}(S_i^q)(Z_{i3}^T(A_{i3}^T P_{i3} + P_{i3}A_{i3} + C_{i1}^T C_{i1})Z_{i3} + Z_{i3}^T P_{i3} B_{i3}\varpi_i^q + (\varpi_i^q)^T B_{i3}^T P_{i3} Z_{i3} - \|\varpi_i^q\|^2) \le -\underline{\lambda}(S_i^q) Z_{i3}^T Q_{i3} Z_{i3}$ and $\dot{V}_1 \le -\underline{\lambda}(Q_{i3})\underline{\lambda}^{\frac12}(P_{i3})/\bar{\lambda}(P_{i3})V_1^{\frac12}$. According to [54], Z_{i3} converges to the origin in a finite time T satisfying $T \le 2\bar{\lambda}(P_{i3})/(\underline{\lambda}(Q_{i3})\underline{\lambda}^{\frac12}(P_{i3}))V_1^{\frac12}(t_0)$.

Similarly, the stability of the RED-based ESO subsystem (39) is given by the following lemma without proof.

Lemma 3: Under Assumption 1, the error dynamics of the RED-based ESO (38) converge to the origin in a finite time, if there exists symmetric positive definite matrices P_{i4} and Q_{i4} such that $A_{i4}^T P_{i4} + P_{i4}A_{i4} + P_{i4}B_{i4}B_{i4}^T P_{i4} + C_{i2}^T C_{i2} = -Q_{i4}$, where $A_{i4} = [-k_{i1}^q/2, 1/2; -k_{i2}^q, 0]$, $B_{i4} = [0; 1]$, and $C_{i2} = [\bar{\sigma}_i^r, 0]$.

The following lemma shows the stability of the closed-loop system (22) and (43).

Lemma 4: Consider the closed-loop system (22) and (43). Under $\|\tilde{\sigma}_i^q\| \le \bar{\sigma}_{ie}^q \in \mathbb{R}^+$ and $|\tilde{\sigma}_i^r| \le \bar{\sigma}_{ie}^r \in \mathbb{R}^+$, the error signals of the closed-loop system are uniformly ultimately bounded with exponential convergence rate for all unknown disturbances σ_i^q and σ_i^r, and any $\psi_i(t_0)$ and $\nu_i(t_0)$.

Proof: Construct a Lyapunov function $V_2 = (V_{i1} + V_{i2})/2$. Taking the derivative of V_2 along (22) and (43), one has

$$\begin{aligned} \dot{V}_2 = & Z_{i1}^T P_{i1}A_{i1}Z_{i1} + Z_{i1}^T P_{i1}B_{i1}(-\tilde{\sigma}_i^q + \tau_i^{q*}) \\ & + Z_{i2}^T P_{i2}A_{i2}Z_{i2} + Z_{i2}^T P_{i2}B_{i2}(-\tilde{\sigma}_i^r + \tau_i^{r*}). \end{aligned} \tag{52}$$

According to (24) and (45), it renders that

$$\begin{aligned} \dot{V}_2 = & (Z_{i1}^T P_{i1}B_{i1}B_{i1}^T P_{i1}Z_{i1} - Z_{i1}^T D_{i1}Q_{i1}D_{i1}Z_{i1})/(2\gamma_{i1}) \\ & + (Z_{i2}^T P_{i2}B_{i2}B_{i2}^T P_{i2}Z_{i2} - Z_{i2}^T D_{i2}Q_{i2}D_{i2}Z_{i2})/(2\gamma_{i2}) \\ & + Z_{i1}^T P_{i1}B_{i1}(\tau_i^{q*} - \tilde{\sigma}_i^q) + Z_{i2}^T P_{i2}B_{i2}(\tau_i^{r*} - \tilde{\sigma}_i^r). \end{aligned} \tag{53}$$

Case I: $\Psi_{i1} > 0$ and $\Psi_{i3} > 0$:

By using the first conditions of (27) and (47), the equation (53) can be rewritten as $\dot{V}_2 = (Z_{i1}^T P_{i1}B_{i1}B_{i1}^T P_{i1}Z_{i1} - Z_{i1}^T D_{i1}Q_{i1}D_{i1}Z_{i1})/(2\gamma_{i1}) + (Z_{i2}^T P_{i2}B_{i2}B_{i2}^T P_{i2}Z_{i2} - Z_{i2}^T D_{i2} Q_{i2}D_{i2}Z_{i2})/(2\gamma_{i2}) - Z_{i1}^T(P_{i1}A_{i1} + A_{i1}^T P_{i1})Z_{i1}/2 - \varrho_{i1}\|Z_{i1}^T P_{i1} B_{i1}\| - Z_{i2}^T(P_{i2}A_{i2} + A_{i2}^T P_{i2})Z_{i2}/2 - \varrho_{i2}\|Z_{i2}^T P_{i2}B_{i2}\| - \epsilon_{i1} V_{i1}/(2\gamma_{i1}) - \epsilon_{i2}V_{i2}/(2\gamma_{i2}) - Z_{i1}^T P_{i1}B_{i1}\tilde{\sigma}_i^q - Z_{i2}^T P_{i2}B_{i2}\tilde{\sigma}_i^r$.

Based on (24) and (45), $\dot{V}_2$ can be deduced as $\dot{V}_2 = -Z_{i1}^T P_{i1}B_{i1}\tilde{\sigma}_i^q - \epsilon_{i1}V_{i1}/(2\gamma_{i1}) - \varrho_{i1}\|Z_{i1}^T P_{i1}B_{i1}\| - Z_{i2}^T P_{i2}B_{i2}\tilde{\sigma}_i^r - \epsilon_{i2}V_{i2}/(2\gamma_{i2}) - \varrho_{i2}\|Z_{i2}^T P_{i2}B_{i2}\|$. From Lemmas 2 and 3, $\tilde{\sigma}_i^q$ and $\tilde{\sigma}_i^r$ are bounded with $\|\tilde{\sigma}_i^q\| \le \bar{\sigma}_{ie}^q$ and $|\tilde{\sigma}_i^r| \le \bar{\sigma}_{ie}^r$. Thus, $\dot{V}_2$ can be represented as follow $\dot{V}_2 \le -\epsilon_{i1}\underline{\lambda}(P_{i1})\|Z_{i1}\|/(2\gamma_{i1}) - \|Z_{i1}^T P_{i1}B_{i1}\|(\varrho_{i1} - \bar{\sigma}_{ie}^q) - \epsilon_{i2}\underline{\lambda}(P_{i2})\|Z_{i2}\|/(2\gamma_{i2}) - \|Z_{i2}^T P_{i2}B_{i2}\|(\varrho_{i2} - \bar{\sigma}_{ie}^r)$.

Case II: $\Psi_{i1} \le 0$ and $\Psi_{i3} \le 0$:

According to the definitions of Ψ_{i1} and Ψ_{i3}, it yields

$$\begin{cases} L_{A_{i1}}V_{i1} + \epsilon_{i1}V_{i1}/\gamma_{i1} + \varrho_{i1}\left\|2Z_{i1}^T P_{i1}B_{i1}\right\| < 0, & \text{(54a)} \\ L_{A_{i2}}V_{i2} + \epsilon_{i2}V_{i2}/\gamma_{i2} + \varrho_{i2}\left\|2Z_{i2}^T P_{i2}B_{i2}\right\| < 0. & \text{(54b)} \end{cases}$$

In this case, $\tau_i^{q*} = 0$ and $\tau_i^{r*} = 0$. Since the second and third terms of (54a) and (54b) are always positive, the negativeness of Ψ_{i1} and Ψ_{i3} stems from $L_{A_{i1}}V_{i1}$ and $L_{A_{i2}}V_{i2}$ to be negative and dominant, respectively. Thus, incorporating (24) and (45) can yield that $P_{i1}B_{i1}B_{i1}^TP_{i1} - D_{i1}Q_{i1}D_{i1} < 0$ and $P_{i2}B_{i2}B_{i2}^TP_{i2} - D_{i2}Q_{i2}D_{i2} < 0$. Then, it gets the positive definite matrices $H_{i1} = D_{i1}Q_{i1}D_{i1} - P_{i1}B_{i1}B_{i1}^TP_{i1}$ and $H_{i2} = D_{i2}Q_{i2}D_{i2} - P_{i2}B_{i2}B_{i2}^TP_{i2}$. With (24) and (45), one has $2P_{i1}A_{i1} = -H_{i1}/\gamma_{i1}$ and $2P_{i2}A_{i2} = -H_{i2}/\gamma_{i2}$. Substituting H_{i1} and H_{i2} into (52) has $\dot{V}_2 \leq -\underline{\lambda}(H_{i1})\|Z_{i1}\|/(2\gamma_{i1}) - \underline{\lambda}(H_{i2})\|Z_{i2}\|/(2\gamma_{i2}) + \|Z_{i1}^TP_{i1}B_{i1}\|\|\bar{\sigma}_{ie}^q\| + \|Z_{i2}^TP_{i2}B_{i2}\|\|\bar{\sigma}_{ie}^r\|$.

The two-sided stability analysis shows that the proposed system is uniformly ultimate bounded. The proof is completed.

B. Safety Analysis

The safety of the proposed multi-ISV system is given by the following lemma.

Lemma 5: Given an under-actuated ISV with dynamics (11), if the optimal control signal τ_i^{q*} belongs to $\mathcal{U}_{i2} \cap \mathcal{U}_{i3}$ for all ISVs, and $p_i(t_0) \in \mathcal{C}_{ij} \cap \mathcal{C}_{io}$, $\forall t > t_0$, $i = 1, \ldots, N$, the networked multi-ISV system is ISSf.

Proof: According to Lemma 1, the set $\mathcal{C}_{ij,1} \cap \mathcal{C}_{ij,2} \cap \mathcal{C}_{io,1} \cap \mathcal{C}_{io,2}$ is forward invariant by using the optimal control signal $\tau_i^{q*} \in \mathcal{U}_{i2} \cap \mathcal{U}_{i3}$, i.e. the set $\mathcal{C}_{ij} \cap \mathcal{C}_{io}$ is ISSF. It shows that if the initial position of all ISVs satisfies $p_i(t_0) \in \mathcal{C}_{ij} \cap \mathcal{C}_{io}$, $i = 1, \ldots, N$, $p_i(t)$ will always stay in $\mathcal{C}_{ij} \cap \mathcal{C}_{io}$. Therefore, the proposed multi-ISV system is ISSf.

The stability and safety of the proposed networked system of multiple ISVs are given by the following theorem.

Theorem 2: Consider a networked system of multiple ISVs with dynamics (11), the distributed motion generator (16), the RED-based ESOs (17) and (38), the stability constraints (26) and (46), the safety constraints (30) and (32), the NLTD (36), the optimal surge force (35) and the optimal yaw moment (49). All error signals of the proposed closed-loop system are uniformly ultimately bounded, and the multi-ISV system is ISSf; i.e. collision avoidance can be ensured.

Proof: According to Lemma 5, each ISV will not violate the safety requirements, i.e., the safety objective (14) and (15) are achieved. Lemma 4 shows that error signals Z_{i1} and Z_{i2} are bounded, and all tracking errors are ultimately bounded, i.e., there exists a positive constant μ such that the geometric objective (13) is achieved.

V. An Application to Vessel Train of Multiple ISVs

This section provides simulation results to verify the effectiveness of the proposed method. The proposed general safety-certified cooperative control architecture is applied to the control of vessel train system consisting of five interconnected ISVs numbered as 1-5 moving along a riverway. In addition, consider one obstructive ISV numbered as 6, one static obstacle numbered as 1 and one dynamic obstacle numbered as 2, shown in Fig. 4.

In order to achieve a fleet formation, each ISV is to track reference signals prescribed by the distributed motion generator (16) based on a consensus scheme as follows $\dot{p}_{1\,d} = q_{1\,d}$, $\dot{q}_{1\,d} = -l_1^2(p_{1\,d} - p_{0\,d} - d_{10}) - 2l_1q_{1\,d}$, $\dot{p}_{2\,d} = q_{2\,d}$, $\dot{q}_{2\,d} = -l_2^2(p_{2\,d} - p_{1\,d} - d_{21}) - 2l_2q_{2\,d}$, $\dot{p}_{3\,d} = q_{3\,d}$, $\dot{q}_{3\,d} = -l_3^2(p_{3\,d} - p_{2\,d} - d_{32}) - 2l_3q_{3\,d}$, $\dot{p}_{4\,d} = q_{4\,d}$, $\dot{q}_{4\,d} = -l_4^2(p_{4\,d} - p_{3\,d} - d_{43}) - 2l_4q_{4\,d}$, $\dot{p}_{5\,d} = q_{5\,d}$, $\dot{q}_{5\,d} = -l_5^2(p_{5\,d} - p_{0\,d} - d_{54}) - 2l_5q_{5\,d}$, where $p_{0\,d} = [t, 0.68t - 30]^T$, $l_1 = l_2 = l_3 = l_4 = l_5 = 2$ and $d_{10} = d_{21} = d_{32} = d_{43} = d_{54} = [-4.4721, -2.2361]^T$. Note that each ISV only communicates with its neighboring ISVs.

Fig. 4. An application to vessel train moving along a riverway.

In this simulation, the five ISVs are scaled-down vehicle model, and the model parameters can be found in [55]. The initial states of five ISVs and the obstructive ISV are set as $\eta_1(0) = [-10, -45, 2\pi/3]^T$, $\eta_2(0) = [-15, -48, 2\pi/3]^T$, $\eta_3(0) = [-20, -50, 2\pi/3]^T$, $\eta_4(0) = [-25, -52, 2\pi/3]^T$, $\eta_5(0) = [-30, -55, 2\pi/3]^T$, $\eta_6(0) = [140, 75, -\pi/2]^T$, $\nu_1(0) = \nu_2(0) = \nu_3(0) = \nu_4(0) = \nu_5(0) = [0, 0, 0]^T$ and $\nu_6(0) = [-0.075, -0.075, 0]^T$, respectively. The initial state of obstacles are set as $p_1(0) = [35, -10]^T$, $q_1(0) = [0, 0]^T$, $p_2(0) = [80, 38]^T$ and $q_2(0) = [0, -0.1]^T$, respectively. The radius of obstacles are assigned as $\rho_1 = 3$ and $\rho_2 = 2$. The safety parameters are selected as $R_c = 6$ and $R_o = 3$. In addition, parameters of the proposed safety-certified cooperative controller are selected as $k_{i1}^q = 2.12$, $k_{i2}^q = 1.1$, $\zeta_i^q = 3.5$, $k_{i1}^r = 2.12$, $k_{i2}^r = 1.1$, $\zeta_i^r = 3.5$, $k_{i1}^\Theta = 4$, $k_{i2}^\Theta = 5.6$, $k_{i3}^\Theta = 1.1$, $\zeta_i^q = 3.5$, $\epsilon_{i3} = 0.366$, $\gamma_{i1} = 4.0$, $\varrho_{i1} = 3.0$, $\epsilon_{i6} = 0.366$, $\gamma_{i2} = 0.5$, $\varrho_{i2} = 1.2$, $\kappa_{i1}(\chi_{ij,0}) = \chi_{ij,0}$, $\kappa_{i2}(\chi_{ij,1}) = \chi_{ij,1}$, $\kappa_{i1}(h_{io}) = h_{io}$, $\kappa_{i2}(\chi_{io}) = \chi_{io}$, $R_c = R_1 = R_2 = 2$, $l_i = 5$, $\varepsilon_i = 0.5$, $\iota_i = 1$.

Figs. 5– 9 show the simulation results. Specifically, Fig. 5 shows the trajectories of five ISVs and the reference trajectories generated by the distributed motion generator. It is seen that a vessel train formation can be achieved by using the proposed safety-certified controller (34) and (49) regardless of the dynamic obstacle, the static obstacle, and the obstructive ISV. Fig. 6 illustrates the collision avoidance process. Specifically, subfigure 6-(a) shows that there is no collision among neighboring ISVs during transient phase $0s \sim 50\,s$; subfigure 6-(b) shows that all ISVs can avoid the static obstacle during $50s \sim 100\,s$; subfigure 6-(c) implies that all ISVs can avoid the dynamic obstacle during $150s \sim 225\,s$; subfigure 6-(d) means that all ISVs can avoid the obstructive ISV during $250s \sim 300\,s$. These four subfigures demonstrate that the vessel train formation is safe during the whole sailing process. Fig. 7 depicts the earth-fixed tracking errors of five ISVs, and they exponentially converge to a small neighborhood of the origin. The four regions (a)-(d) in

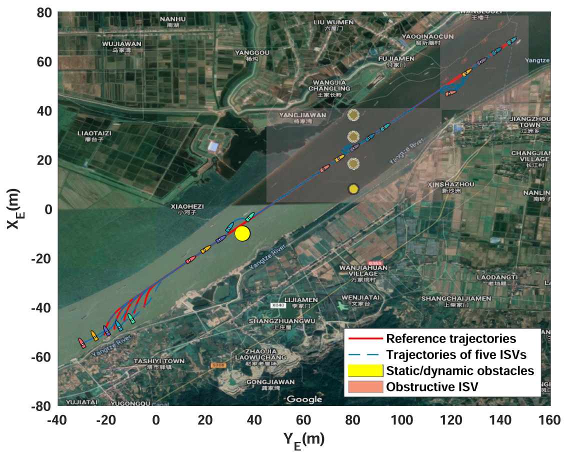

Fig. 5. The fleet trajectories of the five ISVs.

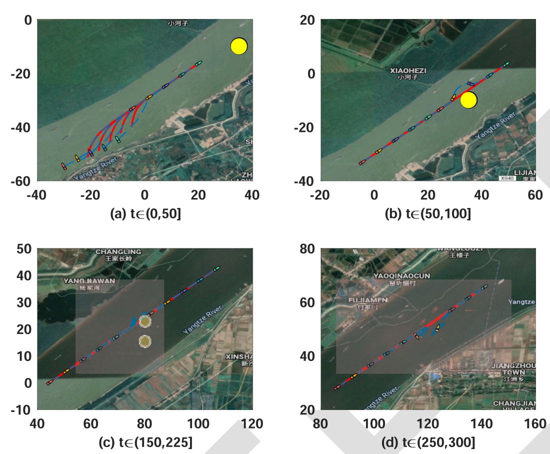

Fig. 6. The snapshots during different collision avoidance processes.

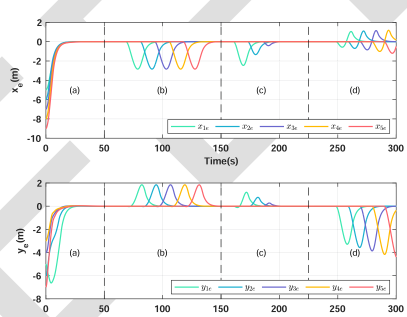

Fig. 7. Tracking errors of five ISVs. .

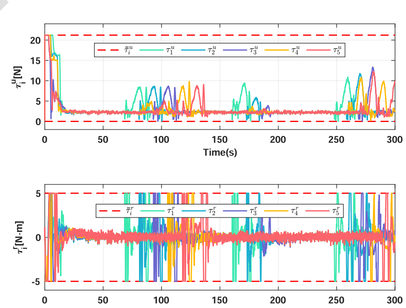

Fig. 8. The optimal surge force and yaw moment.

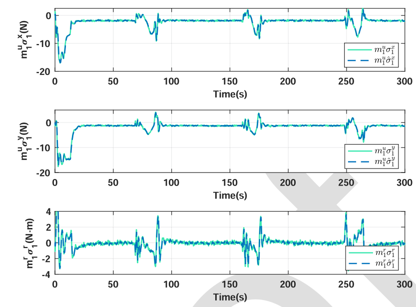

Fig. 9. The earth-fixed total disturbances.

Fig. 7 are consistent with the four subfigures in Fig. 6. It is also observed that the tracking errors become large because the safety objectives (14) and (15) take a higher priority than the geometric objective (13). Fig. 8 presents the optimal surge force and the optimal yaw moment within input constraints. The surge force and yaw moment tunes to satisfy the stability constraints (26) and (46), safety constraints (30) and (32) during the whole control process. Fig. 9 displays the estimation performance for the unknown total disturbances by using the proposed RED-based ESOs (17) and (38), and it can be seen that the total disturbance can be estimated accurately.

VI. Conclusion

This paper presents a general safety-certified cooperative control architecture for a fleet of under-actuated ISVs in the presence of multiple static/dynamic obstacles, in addition to model uncertainties, environmental disturbances, and input constraints. RED-based ESOs are designed for recovering unknown total disturbances in finite time. Based on CLF, ISSf-HOCBF and RED-based ESOs, optimal surge force and yaw moment are obtained by solving the constrained QPs subject to input, stability, safety constraints. One-layer RNNs are employed to solve the quadratic optimization problem on board, which enables real-time implementations without resorting to optimization tools. All tracking errors of the closed-loop system are proven to be uniformly ultimately bounded and the multi-ISV system is proven to be ISSf. Simulation results substantiate the effectiveness of the proposed general safety-certified cooperative control architecture.

References

[1] Z. Peng, J. Wang, D. Wang, and Q. Han, "An overview of recent advances in coordinated control of multiple autonomous surface vehicles," *IEEE Trans. Ind. Informat.*, vol. 17, no. 2, pp. 732–745, Feb. 2021.

[2] S. Xiao, X. Ge, Q.-L. Han, and Y. Zhang, "Resource-efficient platooning control of connected automated vehicles over VANETs," *IEEE Trans. Intell. Veh.*, to be published, doi: 10.1109/TIV.2022.3155640.

[3] X.-M. Zhang *et al.*, "Networked control systems: A survey of trends and techniques," *IEEE/CAA J. Automatica Sinica*, vol. 7, no. 1, pp. 1–17, Jan. 2020.

[4] I. Ahmad, X. Ge, and Q.-L. Han, "Communication-constrained active suspension control for networked in-wheel motor-driven electric vehicles with dynamic dampers," *IEEE Trans. Intell. Veh.*, to be published, doi: 10.1109/TIV.2022.3160165.

[5] X. Wang, "Active fault tolerant control for unmanned underwater vehicle with actuator fault and guaranteed transient performance," *IEEE Trans. Intell. Veh.*, vol. 6, no. 3, pp. 470–479, Sep. 2021.

[6] A. Vagale, R. Oucheikh, R. T. Bye, O. L. Osen, and T. I. Fossen, "Path planning and collision avoidance for autonomous surface vehicles I: A review," *J. Mar. Sci. Technol.*, vol. 26, pp. 1292–1306, 2021.

[7] J. Zhang, L. Pan, Q.-L. Han, C. Chen, S. Wen, and Y. Xiang, "Deep learning based attack detection for cyber-physical system cybersecurity: A survey," *IEEE/CAA J. Autom. Sinica*, vol. 9, no. 3, pp. 377–391, Mar. 2022.

[8] Z. Gao and G. Guo, "Command filtered finite/fixed-time heading tracking control of surface vehicles," *IEEE/CAA J. Autom. Sinica*, vol. 8, no. 10, pp. 1667–1676, Oct. 2021.

[9] K. D. Do, "Bounded controllers for formation stabilization of mobile agents with limited sensing ranges," *IEEE Trans. Autom. Control*, vol. 52, no. 3, pp. 569–576, Mar. 2007.

[10] Y. Dong and S. Xu, "A novel connectivity-preserving control design for rendezvous problem of networked uncertain nonlinear systems," *IEEE Trans. Neural Netw. Learn. Syst.*, vol. 31, no. 12, pp. 5127–5137, Dec. 2020.

[11] S. S. Ge, X. Liu, C. Goh, and L. Xu, "Formation tracking control of multiagents in constrained space," *IEEE Trans. Control Syst. Technol.*, vol. 24, no. 3, pp. 992–1003, May 2016.

[12] Z. Peng, J. Wang, and D. Wang, "Distributed maneuvering of autonomous surface vehicles based on neurodynamic optimization and fuzzy approximation," *IEEE Trans. Control Syst. Technol.*, vol. 26, no. 3, pp. 1083–1090, May 2018.

[13] W. Wu, Z. Peng, D. Wang, L. Liu, and N. Gu, "Anti-disturbance leader-follower synchronization control of marine vessels for underway replenishment based on robust exact differentiators," *Ocean Eng.*, vol. 248, 2022, Art. no. 110686.

[14] S. He, M. Wang, S. Dai, and F. Luo, "Leader-follower formation control of USVs with prescribed performance and collision avoidance," *IEEE Trans. Ind. Informat.*, vol. 15, no. 1, pp. 572–581, Jan. 2019.

[15] S.-L. Dai, S. He, H. Cai, and C. Yang, "Adaptive leader-follower formation control of underactuated surface vehicles with guaranteed performance," *IEEE Trans. Syst., Man, Cybern. Syst.*, vol. 52, no. 3, pp. 1997–2008, Mar. 2022.

[16] Z. Peng, D. Wang, T. Li, and M. Han, "Output-feedback cooperative formation maneuvering of autonomous surface vehicles with connectivity preservation and collision avoidance," *IEEE Trans. Cybern.*, vol. 50, no. 6, pp. 2527–2535, Jun. 2020.

[17] Z. Peng, L. Liu, and J. Wang, "Output-feedback flocking control of multiple autonomous surface vehicles based on data-driven adaptive extended state observers," *IEEE Trans. Cybern.*, vol. 51, no. 9, pp. 4611–4622, Sep. 2021.

[18] N. Gu, D. Wang, Z. Peng, and L. Liu, "Observer-based finite-time control for distributed path maneuvering of underactuated unmanned surface vehicles with collision avoidance and connectivity preservation," *IEEE Trans. Syst., Man, Cybern. Syst.*, vol. 51, no. 8, pp. 5105–5115, Aug. 2019.

[19] B. Wang, S. Nersesov, and H. Ashrafiuon, "Robust formation control and obstacle avoidance for heterogeneous underactuated surface vessel networks," *IEEE Trans. Control Netw. Syst.*, to be published, doi: 10.1109/TCNS.2022.3141022.

[20] G. Zhang, Y. Deng, and W. Zhang, "Robust neural path-following control for underactuated ships with the DVS obstacles avoidance guidance," *Ocean Eng.*, vol. 143, pp. 198–208, 2017.

[21] Q. Zhang, W. Pan, and V. Reppa, "Model-reference reinforcement learning for collision-free tracking control of autonomous surface vehicles," *IEEE Trans. Intell. Transp. Syst.*, to be published, doi: 10.1109/TITS.2021.3086033.

[22] B. S. Park and S. J. Yoo, "An error transformation approach for connectivity-preserving and collision-avoiding formation tracking of networked uncertain underactuated surface vessels," *IEEE Trans. Cybern.*, vol. 49, no. 8, pp. 2955–2966, Aug. 2018.

[23] B. S. Park and S. J. Yoo, "Connectivity-maintaining and collision-avoiding performance function approach for robust leader-follower formation control of multiple uncertain underactuated surface vessels," *Automatica*, vol. 127, 2021, Art. no. 109501.

[24] J. Ghommam, M. Saad, F. Mnif, and Q. M. Zhu, "Guaranteed performance design for formation tracking and collision avoidance of multiple USVs with disturbances and unmodeled dynamics," *IEEE Syst. J.*, vol. 15, no. 3, pp. 4346–4357, Sep. 2020.

[25] X. Sun and S. S. Ge, "Adaptive neural region tracking control of multi-fully actuated ocean surface vessels," *IEEE/CAA J. Autom. Sinica*, vol. 1, no. 1, pp. 77–83, Jan. 2014.

[26] K. D. Do, "Synchronization motion tracking control of multiple underactuated ships with collision avoidance," *IEEE Trans. Ind. Electron.*, vol. 63, no. 5, pp. 2976–2989, May 2016.

[27] Y. Cho, J. Kim, and J. Kim, "Intent inference-based ship collision avoidance in encounters with rule-violating vessels," *IEEE Robot. Automat. Lett.*, vol. 7, no. 1, pp. 518–525, Jan. 2022.

[28] Y. Jiang, Z. Peng, D. Wang, Y. Yin, and Q.-L. Han, "Cooperative target enclosing of ring-networked under-actuated autonomous surface vehicles based on data-driven fuzzy predictors and extended state observers," *IEEE Trans. Fuzzy Syst.*, to be published, doi: 10.1109/TFUZZ.2021.3087920.

[29] Y. Zhao, Y. Ma, and S. Hu, "USV formation and path-following control via deep reinforcement learning with random braking," *IEEE Trans. Neural Netw. Learn. Syst.*, vol. 32, no. 12, pp. 5468–5478, Dec. 2021.

[30] L. Ma, Y.-L. Wang, and Q.-L. Han, "Cooperative target tracking of multiple autonomous surface vehicles under switching interaction topologies," *IEEE/CAA J. Autom. Sinica*, to be published, doi: 10.1109/JAS.2022.105509.

[31] T. Li, R. Zhao, C. L. P. Chen, L. Fang, and C. Liu, "Finite-time formation control of under-actuated ships using nonlinear sliding mode control," *IEEE Trans. Cybern.*, vol. 48, no. 11, pp. 3243–3253, Nov. 2018.

[32] B. Liu, H.-T. Zhang, H. Meng, D. Fu, and H. Su, "Scanning-chain formation control for multiple unmanned surface vessels to pass through water channels," *IEEE Trans. Cybern.*, vol. 52, no. 3, pp. 1850–1861, Mar. 2022.

[33] Z. Peng, J. Wang, and D. Wang, "Containment maneuvering of marine surface vehicles with multiple parameterized paths via spatial-temporal decoupling," *IEEE/ASME Trans. Mechatronics*, vol. 22, no. 2, pp. 1026–1036, Apr. 2017.

[34] L. Liu, D. Wang, Z. Peng, and T. Li, "Modular adaptive control for LOS-based cooperative path maneuvering of multiple underactuated autonomous surface vehicles," *IEEE Trans. Syst., Man, Cybern. Syst.*, vol. 47, no. 7, pp. 1613–1624, Jul. 2017.

[35] Z. Peng, J. Wang, and D. Wang, "Distributed containment maneuvering of multiple marine vessels via neurodynamics-based output feedback," *IEEE Trans. Ind. Electron.*, vol. 64, no. 5, pp. 3831–3839, May 2017.

[36] Q. Zhang, L. Lapierre, and X. Xiang, "Distributed control of coordinated path tracking for networked nonholonomic mobile vehicles," *IEEE Trans. Ind. Informat.*, vol. 9, no. 1, pp. 472–484, Feb. 2013.

[37] N. Gu, Z. Peng, D. Wang, Y. Shi, and T. Wang, "Antidisturbance coordinated path following control of robotic autonomous surface vehicles: Theory and experiment," *IEEE/ASME Trans. Mechatronics*, vol. 24, no. 5, pp. 2386–2396, Oct. 2019.

[38] L. Qiao and W. Zhang, "Trajectory tracking control of AUVs via adaptive fast nonsingular integral terminal sliding mode control," *IEEE Trans. Ind. Informat.*, vol. 16, no. 2, pp. 1248–1258, Feb. 2020.

[39] L. Qiao and W. Zhang, "Double-loop integral terminal sliding mode tracking control for UUVs with adaptive dynamic compensation of uncertainties and disturbances," *IEEE J. Ocean. Eng.*, vol. 44, no. 1, pp. 29–53, Jan. 2019.

[40] L. Liu, D. Wang, and Z. Peng, "ESO-based line-of-sight guidance law for path following of underactuated marine surface vehicles with exact sideslip compensation," *IEEE J. Ocean. Eng.*, vol. 42, no. 2, pp. 477–487, Apr. 2017.

[41] S. Wang and J. Huang, "Cooperative output regulation of singular multi-agent systems under switching network by standard reduction," *IEEE Trans. Circuits Syst. I, Regular Papers*, vol. 65, no. 4, pp. 1377–1385, Apr. 2017.

[42] X. Ge, S. Xiao, Q.-L. Han, X.-M. Zhang, and D. Ding, "Dynamic event-triggered scheduling and platooning control co-design for automated vehicles over vehicular ad-hoc networks," *IEEE/CAA J. Autom. Sinica*, vol. 9, no. 1, pp. 31–46, Jan. 2021.

[43] Y. Huang, S. Z. Yong, and Y. Chen, "Stability control of autonomous ground vehicles using control-dependent barrier functions," *IEEE Trans. Intell. Veh.*, vol. 6, no. 4, pp. 699–710, Dec. 2021.

[44] S. Wang and J. Huang, "Adaptive leader-following consensus for multiple euler-lagrange systems with an uncertain leader system," *IEEE Trans. Neural Netw. Learn. Syst.*, vol. 30, no. 7, pp. 2188–2196, Jul. 2018.

[45] X. Ge, Q.-L. Han, J. Wang, and X.-M. Zhang, "A scalable adaptive approach to multi-vehicle formation control with obstacle avoidance," *IEEE/CAA J. Autom. Sinica*, to be published, doi: 10.1109/JAS.2021.1004263.

[46] Y. Chen, C. Hu, and J. Wang, "Motion planning with velocity prediction and composite nonlinear feedback tracking control for lane-change strategy of autonomous vehicles," *IEEE Trans. Intell. Veh.*, vol. 5, no. 1, pp. 63–74, Mar. 2019.

[47] W. Wu, Z. Peng, D. Wang, L. Liu, and Q.-L. Han, "Network-based line-of-sight path tracking of underactuated unmanned surface vehicles with experiment results," *IEEE Trans. Cybern.*, to be published, doi: 10.1109/TCYB.2021.3074396.

[48] R. Rout, R. Cui, and Z. Han, "Modified line-of-sight guidance law with adaptive neural network control of underactuated marine vehicles with state and input constraints," *IEEE Trans. Control Syst. Technol.*, vol. 28, no. 5, pp. 1902–1914, Sep. 2020.

[49] S. Kolathaya and A. D. Ames, "Input-to-state safety with control barrier functions," *IEEE Contr. Syst. Lett.*, vol. 3, no. 1, pp. 108–113, Jan. 2019.

[50] N. Gu, D. Wang, Z. Peng, J. Wang, and Q.-L. Han, "Disturbance observers and extended state observers for marine vehicles: A survey," *Control Eng. Pract.*, vol. 123, 2022, Art. no. 105158, doi: 10.1016/j.conengprac.2022.105158.

[51] A. D. Ames, K. Galloway, K. Sreenath, and J. W. Grizzle, "Rapidly exponentially stabilizing control lyapunov functions and hybrid zero dynamics," *IEEE Trans. Autom. Control*, vol. 59, no. 4, pp. 876–891, Apr. 2014.

[52] G. Li, Z. Yan, and J. Wang, "A one-layer recurrent neural network for constrained nonsmooth invex optimization," *Neural Netw.*, vol. 50, pp. 79–89, 2014.

[53] T. Sanchez, J. A. Moreno, and L. M. Fridman, "Output feedback continuous twisting algorithm," *Automatica*, vol. 96, pp. 298–305, 2018.

[54] Y. Hong, J. Huang, and Y. Xu, "On an output feedback finite-time stabilization problem," *IEEE Trans. Autom. Control*, vol. 46, no. 2, pp. 305–309, Feb. 2001.

[55] R. Skjetne, T. I. Fossen, and P. V. Kokotović, "Adaptive maneuvering, with experiments, for a model ship in a marine control laboratory," *Automatica*, vol. 41, no. 2, pp. 289–298, 2005.

Wentao Wu (Student Member, IEEE) received the B.E. degree in electrical engineering and automation from the Harbin University of Science and Technology, Harbin, China, in 2018 and the M.E. degree in electrical engineering from Dalian Maritime University, Dalian, China, in 2021. He is currently working toward the Ph.D. degree in electronic information from Shanghai Jiao Tong University, Shanghai, China. His research interests include guidance and control of unmanned surface vehicles.

Zhouhua Peng (Senior Member, IEEE) received the B.E. degree in electrical engineering and automation, the M.E. degree in power electronics and power drives, and the Ph.D. degree in control theory and control engineering from Dalian Maritime University, Dalian, China, in 2005, 2008, and 2011, respectively.

In December 2011, he joined the School of Marine Engineering, Dalian Maritime University, where he is currently a Professor with the School of Marine Electrical Engineering. From July 2014 to April 2018, he was a Postdoctoral Research Fellow with the School of Control Science and Engineering, Dalian University of Technology. From February 2016 to February 2018, he was a Hong Kong Scholar with the Department of Computer Science, City University of Hong Kong, Hong Kong. From January 2019 to February 2019 and from July 2019 to August 2019, he was a Senior Research Fellow with the Department of Computer Science, City University of Hong Kong. He is the author of more than 220 refereed publications. His research focuses on coordinated control of unmanned surface vehicles.

Prof. Peng was the recipient of the Science and Technology Award (First Class) from China Association of Oceanic Engineering in 2019, the natural science awards (Second Class) from Liaoning Province in 2013 and 2017, the Hong Kong Scholar Award in 2016, and the Science and Technology Award for Youth from China Institute of Navigation in 2017. He won the honor of the Young Talent in Science and Technology from the Ministry of Transport of the People's Republic of China in 2017, the Distinguished Young Talent in Science and Technology from Dalian in 2018, and the Bai-Qian-Wan Talent (level Bai) from Liaoning Province in 2019. He is an Associate Editor of the IEEE TRANSACTIONS ON SYSTEMS, MAN, AND CYBERNETICS: SYSTEMS. He also serves on the Editorial Board of the *Chinese Journal of Ship Research*, and the Early Career Advisory Board of IEEE/CAA JOURNAL OF AUTOMATICA SINICA.

Lu Liu (Member, IEEE) received the B.E. degree in electrical engineering and automation and the Ph.D. degree in marine electrical engineering from Dalian Maritime University, Dalian, China, in 2012 and 2018, respectively.

In 2018, she joined the School of Marine Engineering, Dalian Maritime University, where she is currently an Associate Professor with the School of Marine Electrical Engineering and a Postdoctoral Research Fellow with the School of Electrical Information and Electric Engineering, Shanghai Jiao Tong University, Shanghai, China. She has authored more than 40 refereed publications. Her research interests include guidance and control of single/multiple marine surface vehicles.

Dan Wang (Senior Member, IEEE) received the B.E. degree in industrial automation engineering from the Dalian University of Technology, Dalian, China, in 1982, the M.E. degree in marine automation engineering from Dalian Maritime University, Dalian, China, in 1987, and the Ph.D. degree in mechanical and automation engineering from The Chinese University of Hong Kong, Hong Kong, in 2001.

He is currently a Professor with the School of Marine Electrical Engineering, Dalian Maritime University. From November 2001 to October 2005, he was a Research Scientist with Temasek Laboratories, National University of Singapore, Singapore. From January 2012 to May 2012, he was a Visiting Professor with the Institute for Aerospace Studies, University of Toronto, Toronto, ON, Canada. He is the author of more than 260 refereed publications. His research interests include nonlinear system control theory, adaptive control, multiagent system control, and the applications in marine vehicles. Prof. Wang was the recipient of two natural science awards (Second Class) from the Government of Liaoning Province in 2013 and 2017, respectively, and the Science and Technology Award (First Class) from China Association of Oceanic Engineering in 2019. He has served on the committees of many IEEE sponsored conferences as the conference committee Co-Chair, Program Chair, and the Organizing Chair.

A General Safety-Certified Cooperative Control Architecture for Interconnected Intelligent Surface Vehicles With Applications to Vessel Train

Wentao Wu, *Student Member, IEEE*, Zhouhua Peng, *Senior Member, IEEE*, Lu Liu, *Member, IEEE*, and Dan Wang, *Senior Member, IEEE*

***Abstract*—This paper considers cooperative control of interconnected intelligent surface vehicles (ISV) moving in a complex water surface containing multiple static/dynamic obstacles. Each ISV is subject to control force and moment constraints, in addition to internal model uncertainties and external disturbances induced by wind, waves and currents. A general safety-certified cooperative control architecture capable of achieving various collective behaviors such as consensus, containment, enclosing, and flocking, is proposed. Specifically, a distributed motion generator is used to generate desired reference signals for each ISV. Robust-exact-differentiators-based (RED-based) extended state observers (ESOs) are designed for recovering unknown total disturbances in finite time. With the aid of control Lyapunov functions, input-to-state safe high order control barrier functions and RED-based ESOs, constrained quadratic optimization problems are formulated to generate optimal surge force and yaw moment without violating the input, stability, safety constraints. In order to facilitate real-time implementations, a one-layer recurrent neural network is employed to solve the constrained quadratic optimization problem on board. It is proved that all tracking errors of the closed-loop system are uniformly ultimately bounded and the multi-ISV system is input-to-state safe. An example is given to substantiate the effectiveness of the proposed general safety-certified cooperative control architecture.**

***Index Terms*—Distributed motion generator, intelligent surface vehicles, input-to-state safe high-order control barrier function, one-layer recurrent neural networks.**

Manuscript received March 7, 2022; revised April 5, 2022; accepted April 16, 2022. This work was supported in part by the National Natural Science Foundation of China under Grants 51979020, 51909021, 51939001, and 52071044, in part by the Top-notch Young Talents Program of China under Grant 36261402, in part by Liaoning Revitalization Talents Program under Grant XLYC2007188, in part by the Science and Technology Fund for Distinguished Young Scholars of Dalian under Grant 2018RJ08, in part by the Basic Scientific Research in Colleges and Universities of Liaoning Provincial Education Department under Grant LJKQZ2021007, and in part by the Fundamental Research Funds for the Central Universities. *(Corresponding author: Zhouhua Peng.)*

Wentao Wu and Lu Liu are with the School of Marine Electrical Engineering, Dalian Maritime University, Dalian 116026, China, and also with the Department of Automation, Shanghai Jiao Tong University, Shanghai 200240, China (e-mail: wentao-wu@sjtu.edu.cn; luliu@dlmu.edu.cn).

Zhouhua Peng and Dan Wang are with the School of Marine Electrical Engineering, Dalian Maritime University, Dalian 116026, China (e-mail: zhpeng@dlmu.edu.cn; dwang@dlmu.edu.cn).

Color versions of one or more figures in this article are available at https://doi.org/10.1109/TIV.2022.3168974.

Digital Object Identifier 10.1109/TIV.2022.3168974

I. Introduction

With the rapid advancements in communication and computer technologies, cooperative operations of multiple intelligent vehicles has aroused plentiful interest worldwide [1]–[5]. Intelligent surface vehicles (ISV) is a marine transportation platform with numerous applications such as carriage of goods, conveying of passengers and waterway transportation [6]–[8]. A number of cooperative control approaches are proposed such as virtual structure mechanisms [9], behavioral methods [10], artificial potential fields [11], graph-based methods [12], and leader-follower approaches [13].

Various cooperative control approaches for multiple ISVs are proposed; see the references and therein [14]–[27]. Specifically, in [14], [15], leader-follower formation control methods with predefined transient properties are devised for ISVs with the ability of collision avoidance. In [16], an output-feedback consensus maneuvering control method is investigated for a fleet of ISVs, which addresses a cooperative time-varying formation maneuvering problem with connectivity preservation and collision avoidance. In [17], an output-feedback flocking control method is developed for marine vehicles based on data-driven adaptive extended state observers (ESOs). In [18], an observer-based finite-time containment control method is proposed to achieve a path-guided formation capable of avoidance collision and connectivity preservation. In [19], a distributed robust collision-free formation control scheme based on the super-twisting control and persistent excitation is developed for underactuated vessels, which may possess completely different dynamic models. In [20], an improved real-time attitude guidance scheme with the dynamical virtual ship is initially developed for the waypoints-based path-following of ISVs subject to multi-static or slow time-varying obstacles. In [21], a model-reference collision-free tracking control method is presented for surface vehicles to enhance control accuracy and intelligence by using the reinforcement learning technique. In [22], a new nonlinearly transformed formation error is constructed for ISVs to achieve the connectivity preservation, the collision avoidance, and the distributed formation without switching the desired formation pattern and using any additional potential functions. In [23], a robust leader-follower formation tracking algorithm is presented by using connectivity-maintaining and collision-avoiding performance functions for vessels with range-limited communication and completely unknown nonlinearities. In [24], the local path replanning-based repulsive potential function technique is designed to achieve the collision-free distributed formation control with the distributed fixed-time estimator. In [25], a target region tracking control strategy based on the adaptive neural network (NN) is proposed for ocean vessels without no intra-group collisions. In [26], a distributed synchronization controller based on p-times differentiable step functions is designed for multiple ISVs while ensuring no collisions among neighboring ships. In [27], an intent inference-based probabilistic velocity obstacle method is developed to avoid COLREG-violating vessels by combining the marine traffic rules with the proactive evasive actions. However, the formation control methods presented in [7]–[9], [12]–[27] are designed for specific formation scenarios with different control architectures, which may be inflexible in practice one one hand. On the other hand, the collision avoidance methods presented in [14]–[27] cannot avoid collisions with static obstacles, dynamic obstacles, and the neighboring vehicles, simultaneously.

In this paper, we present a general collision-free safety-certified cooperative control architecture for multiple interconnected ISVs subject to input constraints, model uncertainties and environmental disturbances. The cooperative control architecture includes a high-level distributed motion generator and a low-level trajectory tracking controller. Specifically, the distributed motion generator prescribes the reference trajectories for achieving desired swarm behaviors including consensus, containment, enclosing, flocking, etc. At the low level control, by using robust-exact-differentiator-based (RED-based) ESOs for estimating the total disturbances in finite time, control Lyapunov functions (CLF) for assuring stability, and input-to-state safe high order control barrier functions (ISSf-HOCBF) for guaranteeing safety, constrained quadratic programs (QPs) are formulated to obtain optimal surge force and yaw moment. To facilitate real-time implementations, one-layer recurrent neural networks (RNNs) are employed to solve the constrained quadratic optimization problem on board. The tracking errors of the closed-loop system are proved to be uniformly ultimately bounded and the safety of the multi-ISV system is guaranteed. An application to the vessel train is given to substantiate the effectiveness of the proposed general safety-certified cooperative control architecture.

Compared with contributions in [7]–[9], [12]–[48], the main features of the proposed general safety-certified cooperative control architecture with control method are summarized into three-folds:

1) In contrast to the formation controllers in [7]–[9], [12]–[44] with specific coordinated control scenarios, this paper presents a general safety-certified cooperative control architecture consisting of a high-level distributed motion generator and a low-level tracking controller. The proposed cooperative control architecture is universal and takes the capabilities to be compatible with various coordinated control scenarios and achieve various collective behaviors.
2) In contrast to the collision avoidance strategies in [14]–[27], [45], [46], ISSf-HOCBFs are designed to construct the safety constraints from static/dynamic obstacles and neighboring vehicles. Within safety, stability, and input constraints, the optimal control force and moment are obtained in realtime by the designed RNNs without resorting to optimization tools.
3) In contrast to the disturbance observers in [16], [17], [26], [34], [47], the proposed RED-based ESOs can estimate the unknown total disturbances in finite time. Different from the fuzzy/NN approximation approaches in [14], [15], [20], [21], [24], [25], [28], [33], [35], [48], RED-based ESOs takes a simpler estimation structure and fewer tuning parameters.

This paper is organized as follows. Section II states preliminaries and problem formulation. Section III designs the controller. Section IV analyzes the stability and the safety of the closed-loop system. Section V gives simulation results. Section VI concludes this paper.

II. Preliminaries and Problem Formulation

A. Notation

For a vector $a = [a_1, \ldots, a_n]^T \in \mathbb{R}^n$ and a constant $b \in (0, 1)$, we define the symbol $\lceil a \rfloor^b = [\lceil a_1 \rfloor^b, \ldots, \lceil a_n \rfloor^b]^T$ with $\lceil a_i \rfloor^b = \mathrm{sgn}(a_i)|a_i|^b$, $i = 1, \ldots, n$, where $\mathrm{sgn}(\cdot)$ is a signum function. A continuous function $\kappa(\cdot) : (c, d) \mapsto \mathbb{R}$ is named as an extended class $\mathcal{K}$ function ($\kappa(\cdot) \in \mathcal{K}_e$) with $c, d > 0$, iff $\kappa(\cdot)$ is strictly monotonically increasing and $\kappa(0) = 0$. It is called as an extended class $\mathcal{K}_\infty$ function ($\kappa(\cdot) \in \mathcal{K}_{\infty,e}$) when $c, d \mapsto \infty$ and $\lim_{\iota \mapsto \infty} \kappa(\iota) = \infty$, $\lim_{\iota \mapsto -\infty} \kappa(\iota) = -\infty$. ess sup $(\cdot)$ denotes the essential supremum of $(\cdot)$.

B. Input-to-State Safe High Order Control Barrier Function

Consider an affine control system with disturbances $\omega \in \mathbb{R}^n$ in this form

$$\dot{x} = f(x) + g(x)u + \omega, \tag{1}$$

where $x \in \mathbb{R}^n$ is the system state. $u \in \mathbb{R}^m$ is the control input. $f(x) \in \mathbb{R}^n$ and $g(x) \in \mathbb{R}^{n\times m}$ are locally Lipschitz continuous functions. ω is assumed to be bounded and satisfied with $\|\omega\|_\infty \triangleq \mathrm{ess\,sup}_{t>0} \|\omega\|$.

Definition 1 ([49]): For a system (1) with $\omega = 0$, a super-level set $\mathcal{C} \subset \mathbb{R}^n$ with a continuously differentiable function $h(x) : \mathbb{R}^n \mapsto \mathbb{R}$ is defined as

$$\begin{aligned} \mathcal{C} &= \{x \in \mathbb{R}^n : h(x) \geq 0\},\\ \partial\mathcal{C} &= \{x \in \mathbb{R}^n : h(x) = 0\},\\ \mathrm{Int}(\mathcal{C}) &= \{x \in \mathbb{R}^n : h(x) > 0\}. \end{aligned} \tag{2}$$

Then, the set $\mathcal{C}$ is forward invariant if there is $x(t) \in \mathcal{C}$ for any $x(t_0) \in \mathcal{C}$, $\forall\, t \geq t_0$. The forward invariance of $\mathcal{C}$ indicates that the system (1) with $\omega = 0$ is safe on $\mathcal{C}$.

Definition 2 ([49]): For a system (1), an extended set $\mathcal{C}_\omega \supset \mathcal{C}$ with the continuous functions $h(x)$ is defined as follows

$$\begin{aligned} \mathcal{C}_\omega &= \{x \in \mathbb{R}^n : h(x) + \kappa_\omega(\|\omega\|_\infty) \geq 0\},\\ \partial\mathcal{C}_\omega &= \{x \in \mathbb{R}^n : h(x) + \kappa_\omega(\|\omega\|_\infty) = 0\},\\ \mathrm{Int}(\mathcal{C}_\omega) &= \{x \in \mathbb{R}^n : h(x) + \kappa_\omega(\|\omega\|_\infty) > 0\}. \end{aligned} \tag{3}$$

The set $\mathcal{C}_\omega$ is forward invariant for all $\|\omega\|_\infty \le \bar{\omega} \in \mathbb{R}^+$, if there exist a control input u and a function $\kappa_\omega(\cdot) \in \mathcal{K}_\infty$. Then, the system (1) is input-to-state safe (ISSf) on $\mathcal{C}$ as in (2) if the forward invariant set $\mathcal{C}_\omega$ is existed.

For a continuously differentiable function $h(x)$ with a relative degree $d > 1$, we define a series of functions $\chi_i : \mathbb{R}^n \mapsto \mathbb{R}$ and corresponding sets $\mathcal{C}_{i\omega}$ as follows

$$\begin{cases} \chi_i(x) = \dot{\chi}_{i-1}(x) + \kappa_i\left(\chi_{i-1}(x)\right), \\ \mathcal{C}_{i\omega} = \{x \in \mathbb{R}^n : \chi_{i-1}(x) \ge -\kappa_{i\omega}(\|\omega\|_\infty)\}, \end{cases} \tag{4}$$

where $\chi_0(x) = h(x)$, $i = 1, \ldots d$, and $\kappa_i(\cdot) \in \mathcal{K}_{\infty,e}$.

Definition 3 ([49]): Given functions $\chi_1(x), \ldots, \chi_d(x)$ and sets $\mathcal{C}_{1\omega}, \ldots, \mathcal{C}_{d\omega}$ defined by (4), the continuously differentiable function $h(x)$ with relative degree $d > 1$ is called as an ISSf-HOCBF for system (1) on the set $\mathcal{C}$, if there exist a constant $\bar{\omega} > 0$ and functions $\kappa_d(\cdot) \in \mathcal{K}_{\infty,e}$, $\kappa_{d\omega}(\cdot) \in \mathcal{K}_\infty$ such that for all $x \in \mathbb{R}^n$ and $\omega \in \mathbb{R}^n$ with $\|\omega\|_\infty \le \bar{\omega}$

$$\sup_{u \in \mathbb{R}^m} \left[L_f^d h(x) + L_g L_f^{d-1} h(x) u + \frac{\partial \chi_{d-1}(x)}{\partial x^T} \omega + \kappa_d\left(\chi_{d-1}(x)\right) \right] \ge -\kappa_{d\omega}(\|\omega\|_\infty), \tag{5}$$

where $L_f^d h$ and $L_g L_f^{d-1} h$ represent the Lie derivatives of $h(x)$.

Lemma 1 ([49]): Given an ISSf-HOCBF $h(x)$ defined by Def. 3 for system (1) on $\mathcal{C}$, any Lipschitz continuous controller $u \in \mathcal{U}(x)$ for all $x \in \mathbb{R}^n$ satisfying

$$\mathcal{U}(x) = \left\{ u \in \mathbb{R}^m : L_f^d h(x) + L_g L_f^{d-1} h(x) u + \frac{\partial \chi_{d-1}(x)}{\partial x^T} \omega + \kappa_d\left(\chi_{d-1}(x)\right) \ge -\kappa_{d\omega}(\|\omega\|_\infty) \right\} \tag{6}$$

yields that the set $\mathcal{C}_{1\omega} \cap \mathcal{C}_{2\omega} \cap, \ldots, \cap \mathcal{C}_{d\omega}$ is forward invariant, which means that the system (1) is ISSf on $\mathcal{C}$.

Noting that the term ω may be unavailable for a practical system. Hereby, the following theorem is given.

Theorem 1: Given a series of functions $\chi_1(x), \ldots, \chi_d(x)$ and sets $\mathcal{C}_{1\omega}, \ldots, \mathcal{C}_{d\omega}$ defined by (4), the continuously differentiable function $h(x)$ of relative degree $d > 1$ is called as ISSf-HOCBF for the system (1) on the set $\mathcal{C}$, if there exist a constant $\bar{\omega} > 0$ and a function $\kappa_d(\cdot) \in \mathcal{K}_{\infty,e}$ such that for all $x \in \mathbb{R}^n$ and $\omega \in \mathbb{R}^n$ with $\|\omega\|_\infty \le \bar{\omega}$

$$\sup_{u \in \mathbb{R}^m} \left[L_f^d h(x) + L_g L_f^{d-1} h(x) u - \frac{\partial \chi_{d-1}(x)}{\partial x^T} \frac{\partial \chi_{d-1}(x)}{\partial x} + \kappa_d\left(\chi_{d-1}(x)\right) \right] \ge 0. \tag{7}$$

any Lipschitz continuous controller $u \in \mathcal{U}^*(x)$ satisfying

$$\mathcal{U}^*(x) = \left\{ u \in \mathbb{R}^m : L_f^d h(x) + L_g L_f^{d-1} h(x) u - \frac{\partial \chi_{d-1}(x)}{\partial x^T} \frac{\partial \chi_{d-1}(x)}{\partial x} + \kappa_d\left(\chi_{d-1}(x)\right) \ge 0 \right\}. \tag{8}$$

devises the system ISSf on the set $\mathcal{C}$.

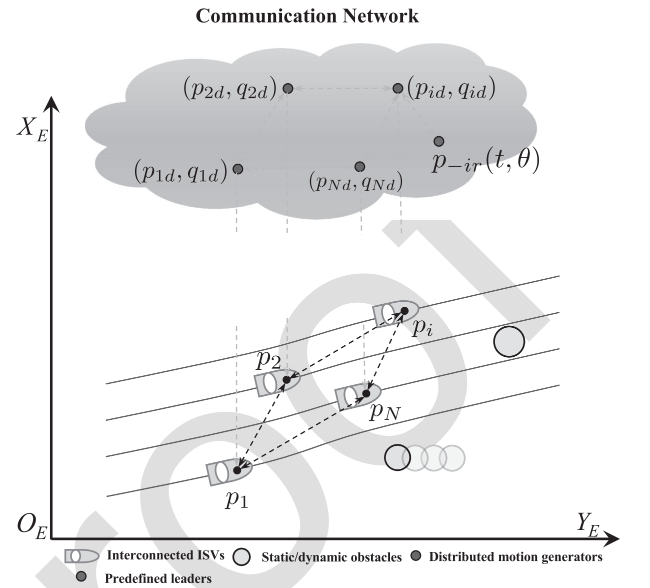

Fig. 1. Cooperative control scenario of ISVs subject to static/dynamic obstacles.

Proof: From (4), taking the derivative of $\chi_d(x)$ yields

$$\dot{\chi}_d = L_f^d h(x) + L_g L_f^{d-1} h(x) u + \frac{\partial \chi_{d-1}}{\partial x^T} \omega + \kappa_d(\chi_{d-1}). \tag{9}$$

For $u \in \mathcal{U}^*(x)$, one has

$$\dot{\chi}_d \ge \left(\left\| \frac{\partial \chi_{d-1}(x)}{\partial x} \right\| - \frac{\|\omega\|}{2} \right)^2 - \frac{\|\omega\|^2}{4} \ge -\frac{\|\omega\|^2}{4}. \tag{10}$$

Obviously, the inequality (10) is in the form of (5). It is concluded that the function $h(x)$ is ISSf-HOCBF of system (1) and the set $\mathcal{U}^*(x)$ satisfies $\mathcal{U}^*(x) \subseteq \mathcal{U}(x)$. It means that Theorem 1 holds. The proof is completed.

C. Problem Formulation

Consider a networked system with N underactuated ISVs shown in Fig. 1. It is assumed that each ISV has a plane of symmetry; heave, pitch, and roll modes are neglected. The kinematic and kinetic dynamics of the ith ISV are described as follows [26]

$$\begin{cases} \dot{\eta}_i = R_i(\psi_i)\nu_i, \\ M_i \dot{\nu}_i = f_i(\nu_i) + \tau_i + \tau_{iw}, \end{cases} \tag{11}$$

where $i = 1, \ldots, N$. $\eta_i = [p_i^T, \psi_i]^T$ denotes the position and yaw angular with $p_i = [x_i, y_i]^T \in \mathbb{R}^2$ and $\psi_i \in (-\pi, \pi]$. $\nu_i = [u_i, v_i, r_i]^T \in \mathbb{R}^3$ represents the body-fixed velocity vector along the surge, sway and yaw direction. $M_i = \mathrm{diag}\{m_i^u, m_i^v, m_i^r\} \in \mathbb{R}^3$ is the inertia mass matrix. $f_i(\nu_i) \in \mathbb{R}^3$ is the unknown function including Coriolis terms, damping terms and unmodeled dynamics. $\tau_i = [\tau_i^u, 0, \tau_i^r]^T$ is a bounded control input satisfying $0 \le \tau_i^u \le \bar{\tau}_i^u$ and $-\bar{\tau}_i^r \le \tau_i^r \le \bar{\tau}_i^r$ with $\bar{\tau}_i^u \in \mathbb{R}^+$ and $\bar{\tau}_i^r \in \mathbb{R}^+$ being bounds of input signals. $\tau_{iw} \in \mathbb{R}^3$ presents the unknown environmental disturbances due to wind, wave and current. $R_i(\psi_i) = \mathrm{diag}\{R_i^p(\psi_i), 1\}$ is a rotation matrix with $R_i^p(\psi_i) = [\cos(\psi_i), -\sin(\psi_i); \sin(\psi_i), \cos(\psi_i)]$.

To design the safety-certified controllers, the model dynamics (11) is rewritten as

$$\begin{cases} \dot{p}_i = q_i, & \text{(12a)}\\ \dot{q}_i = \sigma_i^q + \tau_i^q/m_i^u, & \text{(12b)}\\ \dot{\psi}_i = r_i, & \text{(12c)}\\ \dot{r}_i = \sigma_i^r + \tau_i^r/m_i^r, & \text{(12d)} \end{cases}$$

where $q_i = R_i^p(\psi_i)[u_i, v_i]^T$ and $[\sigma_i^{qT}, \sigma_i^r]^T = \dot{R}_i(\psi_i)\nu_i + R_i(\psi_i)M_i^{-1}(f_i(\nu_i) + \tau_{iw})$ with $\sigma_i^q = [\sigma_i^x, \sigma_i^y]^T \in \mathbb{R}^2$ and $\sigma_i^r \in \mathbb{R}$ being unknown earth-fixed disturbances. $\tau_i^q = [\tau_i^x, \tau_i^y]^T \in \mathbb{R}^2$ stands for the earth-fixed control input satisfying $\tau_i^x = \tau_i^u\cos(\psi_i)$ and $\tau_i^y = \tau_i^u \sin(\psi_i)$.

This paper aims to present a general safety-certified cooperative control architecture for underactuated ISVs subject to static/dynamic obstacles to achieve the following objectives:

1) *Geometric Objective:* Force each ISV to track the reference trajectory $p_{id} = [x_{id}, y_{id}]^T$ such that

$$\|p_i - p_{id}\| < \mu, \tag{13}$$

where $i = 1, \ldots, N$ and $\mu \in \mathbb{R}^+$.

2) *Safety Objective:* To guarantee the safety of multi-ISV system, the following distance constraints are required to be satisfied:

1) Inter-ISV collision avoidance:

$$\|p_i - p_j\| > R_c, \tag{14}$$

where $i, j = 1, \ldots, N, i \neq j$. $R_c \in \mathbb{R}^+$ is the minimum collision-free distance among neighboring ISVs.

2) Obstacle collision avoidance:

$$\|p_i - p_o\| > R_o + \rho_o, \tag{15}$$

where $i = 1, \ldots, N$, $o = 1, \ldots, N_o$ with $N_o \in \mathbb{R}^+$ being the total number of obstacles. $p_o \in \mathbb{R}^2$ presents the position of obstacle. $R_o \in \mathbb{R}^+$ is the minimum collision-free distance from obstacles. $\rho_o \in \mathbb{R}^+$ is the radius of the oth obstacle.

III. General Cooperative Control Architecture

A. High Level Distributed Motion Generator

Based on the vehicle model in (11), a series of distributed cooperative control schemes are presented to achieve various collective behaviors such as consensus [16], containment [18], flocking [17], and enclosing [28]. In [16], [18], [28], the control laws are designed for specific formations. Once the mission is changed, the control law has to be switched. To remedy this limitation, a general safety-certified cooperative control architecture for multiple ISVs is proposed, which are able to achieve various formation without modifying the low-level control laws. As shown in Fig. 2, it includes a high-level motion generator and a low-level trajectory tracking controller. Motivated by the distributed cooperative control laws in for achieving consensus, containment, enclosing, and flocking, a distributed motion generator is proposed as follows

$$\begin{cases} \dot{p}_{id} = q_{id},\\ \dot{q}_{id} = \hbar_i(p_{-ir}(t,\theta), p_{id}, q_{id}, p_{-id}, q_{-id}), \end{cases} \tag{16}$$

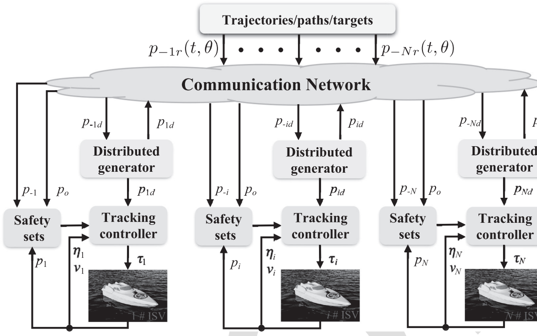

Fig. 2. A general safety-certified cooperative control architecture for ISVs.

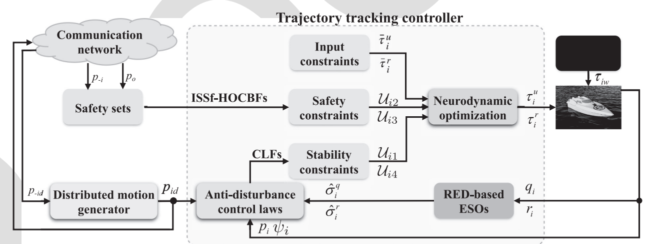

Fig. 3. The low-level safety-certified control architecture.

where $p_{id} \in \mathbb{R}^2$ and $q_{id} \in \mathbb{R}^2$ are the states of the generator. $p_{-ir}(t,\theta) = \{p_{lr}(t,\theta_l)\}_{l\in\mathcal{N}_i^L}$ is the predefined input signal, which may be the trajectory, the path or the target with $\theta_l \in \mathbb{R}$ being a path parameter. p_{-id} and q_{-id} are output signals of the ith generator's neighbors satisfying $p_{-id} = \{p_{kd}\}_{k\in\mathcal{N}_i^F}$ and $q_{-id} = \{q_{kd}\}_{k\in\mathcal{N}_i^F}$. $\hbar_i(\cdot) \in \mathbb{R}^2$ are known, bounded and Lipschitz functions, which can be designed by the specific mission scenarios.

B. Low Level Trajectory Tracking Controller

In this subsection, a safety-certified cooperative control law is developed for ISVs to track the reference trajectory. Fig. 3 presents the block diagram of the proposed low-level controller for the ith ISV.

1) The Optimal Surge Force Controller: The ESO is an effective and appealing tool to address the unknow uncertainties [50]. To estimate the unknown term σ_i^q in (12b), the RED-based ESO is proposed as follows

$$\begin{cases} \dot{\hat{q}}_i = -k_{i1}^q \zeta_i^{q\frac{1}{2}} \lceil \hat{q}_i - q_i \rfloor^{\frac{1}{2}} + \hat{\sigma}_i^q + \tau_i^q/m_i^u,\\ \dot{\hat{\sigma}}_i^q = -k_{i2}^q \zeta_i^q \operatorname{sgn}(\hat{q}_i - q_i), \end{cases} \tag{17}$$

where $\hat{q}_i = [\hat{q}_i^x, \hat{q}_i^y]^T \in \mathbb{R}^2$ and $\hat{\sigma}_i^q = [\hat{\sigma}_i^x, \hat{\sigma}_i^y]^T \in \mathbb{R}^2$ represent the estimated values of q_i and σ_i^q, respectively. k_{i1}^q and k_{i2}^q are positive constants. $\zeta_i^q \in \mathbb{R}^+$ is a scaling factor.

Define the estimated errors $\tilde{q}_i = (\hat{q}_i - q_i)/\zeta_i^q$ and $\tilde{\sigma}_i^q = (\hat{\sigma}_i^q - \sigma_i^q)/\zeta_i^q$. Combining (12a)-(12b) with (17), the time derivatives of $\tilde{q}_i$ and $\tilde{\sigma}_i^q$ are deduced as follows

$$\begin{cases} \dot{\tilde{q}}_i = -k_{i1}^q \lceil \tilde{q}_i \rfloor^{\frac{1}{2}} + \tilde{\sigma}_i^q,\\ \dot{\tilde{\sigma}}_i^q = -k_{i2}^q \operatorname{sgn}(\tilde{q}_i) - \dot{\sigma}_i^q/\zeta_i^q. \end{cases} \tag{18}$$

Letting $z_{i1} = p_i - p_{id}$ and taking its derivative with (12a), (12b), and (16), it yields that

$$\dot{z}_{i1} = q_i - q_{id} \text{ and } \ddot{z}_{i1} = \sigma_i^q + \tau_i^q / m_i^u - \dot{q}_{id}. \tag{19}$$

To stabilize the error dynamics $\ddot{z}_{i1}$, by using the estimated information from RED-based ESO, an anti-disturbance control law is presented as follows

$$\tau_i^q = m_i^u(\dot{q}_{id} + \tau_i^{q*} - \hat{\sigma}_i^q) \tag{20}$$

with $\tau_i^{q*} = [\tau_i^{x*}, \tau_i^{y*}]^T$ being an earth-fixed optimal control signals. Substituting (20) into (19), one has

$$\dot{z}_{i1} = q_i - q_{id} \text{ and } \ddot{z}_{i1} = -\tilde{\sigma}_i^q + \tau_i^{q*}. \tag{21}$$

To obtain optimal surge force τ_i^u, the following constraints are constructed to achieve stability and safety.

Step 1. CLF-based stability constraint

Let $Z_{i1} = [z_{i1}^T, \dot{z}_{i1}^T]^T$ and take its derivative along (21) as

$$\dot{Z}_{i1} = A_{i1} Z_{i1} + B_{i1}(-\tilde{\sigma}_i^q + \tau_i^{q*}) \tag{22}$$

with $A_{i1} = [0_2, I_2; 0_2, 0_2]$ and $B_{i1} = [0_2, I_2]^T$.

To stabilize Z_{i1}, a candidate Lyapunov function V_{i1} is constructed as follows

$$V_{i1} = Z_{i1}^T P_{i1} Z_{i1}, \tag{23}$$

where $P_{i1} = P_{i1}^T$ is a positive-definite matrix such that the continuous algebraic Riccati equation

$$A_{i1}^T P_{i1} + P_{i1} A_{i1} - \frac{P_{i1} B_{i1} B_{i1}^T P_{i1} - D_{i1} Q_{i1} D_{i1}}{\gamma_{i1}} = 0, \tag{24}$$

where γ_{i1} is a positive constant. Q_{i1} represents a symmetric positive-definite matrix and $D_{i1} = [I_2/\gamma_{i1}, 0_2; 0_2, I_2]$.

Apply the transform $P_{i1} = D_{i1} P'_{i1} D_{i1}$, where $P'_{i1} = P'^T_{i1} > 0$ satisfies

$$A_{i1}^T P'_{i1} + P'_{i1} A_{i1} - P'_{i1} B_{i1} B_{i1}^T P'_{i1} + Q_{i1} = 0. \tag{25}$$

Based on the dynamics (22), a CLF-based stability constraint set for the optimal signal τ_i^{q*} is constructed as [51]

$$\mathcal{U}_{i1} = \left\{ \tau_i^{q*} : L_{A_{i1}} V_{i1} + L_{B_{i1}} V_{i1} \tau_i^{q*} + \frac{\epsilon_{i1}}{\gamma_{i1}} V_{i1} \leq 0 \right\}, \tag{26}$$

where $L_{A_{i1}} V_{i1} = Z_{i1}^T (P_{i1} A_{i1} + A_{i1}^T P_{i1}) Z_{i1}$, $L_{B_{i1}} V_{i1} = 2 Z_{i1}^T P_{i1} B_{i1}$ and $\epsilon_{i1} = \lambda_{\min}(Q_{i1}) / \bar{\lambda}(P'_{i1})$.

To calculate the open-loop solution in (26), a position pointwise min-norm control law is developed as follows

$$\tau_i^{q*} = \begin{cases} -\Psi_{i1} \Psi_{i2} / (\Psi_{i2}^T \Psi_{i2}), & \text{if } \Psi_{i1} > 0, \\ 0, & \text{if } \Psi_{i1} \leq 0, \end{cases} \tag{27}$$

where $\Psi_{i1} = L_{A_{i1}} V_{i1} + \epsilon_{i1} V_{i1} / \gamma_{i1} + \varrho_{i1} \| L_{B_{i1}} V_{i1} \|$ and $\Psi_{i2} = L_{B_{i1}} V_{i1}$ with ϱ_{i1} being a positive constant.

Step 2. ISSf-HOCBF-based safety constraints

Substituting (20) into (12b), the dynamic subsystem (12a)-(12b) can be rewritten as follows

$$\dot{e}_i = f_i + g_i \tau_i^{q*} + \omega_i, \tag{28}$$

where $e_i = [p_i^T, q_i^T]^T$, $f_i = [q_i^T, 0_2]^T$, $g_i = [0_2, I_2]^T$ and $\omega_i = [0_2, \dot{q}_{id}^T - \tilde{\sigma}_i^{qT}]^T$.

From Def. 1, safety objectives (14) and (15) are encoded into super-level sets $\mathcal{C}_{ij}$ and $\mathcal{C}_{io}$, respectively. It means that the forward invariance of sets $\mathcal{C}_{ij}$ and $\mathcal{C}_{io}$ are equivalent to the safety of the ith ISV. Then, we aim to devise the control constraint sets for ensuring forward invariance of $\mathcal{C}_{ij}$ and $\mathcal{C}_{io}$.

In order to avoid collision among ISVs, the set $\mathcal{C}_{ij}$ is constructed as follows

$$\mathcal{C}_{ij} = \left\{ p_i \in \mathbb{R}^2 : h_{ij}(p_i) = \|p_{ij}\|^2 - R_c^2 \geq 0 \right\}, \tag{29}$$

where $p_{ij} = p_i - p_j$. $h_{ij}(p_i)$ is a candidate ISSf-HOCBF.

From (4), a family of functions with $h_{ij}(p_i)$ are defined as $\chi_{ij,0} = h_{ij}$, $\chi_{ij,1} = \dot{\chi}_{ij,0} + \kappa_{i1}(\chi_{ij,0})$, $\chi_{ij,2} = \dot{\chi}_{ij,1} + \kappa_{i2}(\chi_{ij,1})$, and the corresponding safety sets are denoted as $\mathcal{C}_{ij,1} = \{p_i \in \mathbb{R}^2 : \chi_{ij,0} \geq \kappa_{i\omega,1}(\|\omega_i\|_\infty)\}$ and $\mathcal{C}_{ij,2} = \{p_i \in \mathbb{R}^2 : \chi_{ij,1} \geq \kappa_{i\omega,2}(\|\omega_i\|_\infty)\}$, where $\kappa_{i1}(\cdot)$, $\kappa_{i2}(\cdot) \in \mathcal{K}$ and $\kappa_{i\omega,1}(\cdot)$, $\kappa_{i\omega,2}(\cdot) \in \mathcal{K}_\infty$.

According to (6) and (28), the safety constraint of the control input for the ith ISV is devised as

$$\mathcal{U}_{i2} = \left\{ \tau_i^{q*} : L_{f_i}^2 h_{ij} + L_{g_i} L_{f_i} h_{ij} \tau_i^{q*} - \frac{\partial \chi_{ij,1}(p_i)}{\partial p_i^T} \frac{\partial \chi_{ij,1}(p_i)}{\partial p_i} + \kappa_{i2}(\chi_{ij,1}) \geq 0 \right\}, \tag{30}$$

where $L_{f_i}^2 h_{ij} = 2(q_i - q_j)^T (q_i - q_j)$ and $L_{g_i} L_{f_i} h_{ij} = 2 p_{ij}^T$.

To avoid collision between ISVs and static/dynamic obstacles, the safe set $\mathcal{C}_{io}$ is developed as follows

$$\mathcal{C}_{io} = \{p_i \in \mathbb{R}^2 : h_{io}(p_i) = \|p_{io}\|^2 - (R_o + \rho_o)^2 \geq 0\} \tag{31}$$

where $p_{io} = p_i - p_o$.

Similarly, the safety constraint with $h_{io}(p_i)$ is described as

$$\mathcal{U}_{i3} = \left\{ \tau_i^{q*} : L_{f_i}^2 h_{io} + L_{g_i} L_{f_i} h_{io} \tau_i^{q*} - \frac{\partial \chi_{ij,1}(p_i)}{\partial p_i^T} \frac{\partial \chi_{ij,1}(p_i)}{\partial p_i} + \kappa_{i2}(\chi_{io}) \geq 0 \right\}, \tag{32}$$

where $L_{f_i}^2 h_{io} = 2(q_i - q_o)^T (q_i - q_o)$, $L_{g_i} L_{f_i} h_{io} = 2 p_{io}^T$, and $\chi_{io} = \dot{h}_{io} + \kappa_{i1}(h_{io})$.

Step 3. QP-based optimal surge force

For the cooperative formation of multiple ISVs, the safety objective has higher priority than the geometric objective. To unify the designed stability constraint (26), safety constraints (30), (32) and input constraints, a quadratic optimization problem is formulated as follows

$$\begin{aligned} \tau_i^{q*} = \underset{[\tau_i^{q*}; \delta_i] \in \mathbb{R}^3}{\operatorname{argmin}} \quad & J_i^q(\tau_i^{q*}) = \|\tau_i^{q*}\|^2 + l_i \delta_i^2 \\ \text{s.t.} \quad & \Psi_{i2}(Z_{i1}) \tau_i^{q*} \leq b_{i1}, \\ & -L_{g_i} L_{f_i} h_{ij} \tau_i^{q*} \leq b_{i2}, \\ & -L_{g_i} L_{f_i} h_{io} \tau_i^{q*} \leq b_{i3}, \\ & \underline{\tau}_i^{q*} \leq \tau_i^{q*} \leq \bar{\tau}_i^{q*}, \end{aligned} \tag{33}$$

where δ_i is a relaxation variable. $l_i \in \mathbb{R}^+$ denotes a penalty coefficient. $b_{i1} = -\Psi_{i1}(Z_{i1}) + \delta_i$, $b_{i2} = L_{f_i}^2 h_{ij} - (\partial \chi_{ij,1}(p_i) / \partial p_i^T)(\partial \chi_{ij,1}(p_i) / \partial p_i) + \kappa_{i2}(\chi_{ij,1})$, $b_{i3} = L_{f_i}^2 h_{io} - (\partial \chi_{ij,1}(p_i) / \partial p_i^T)(\partial \chi_{ij,1}(p_i) / \partial p_i) + \kappa_{i2}(\chi_{io})$, $\bar{\tau}_i^{q*} = \bar{\tau}_i^q / m_i^u + \hat{\sigma}_i^q - \ddot{p}_{id}$ and $\underline{\tau}_i^{q*} = -\bar{\tau}_i^q / m_i^u + \hat{\sigma}_i^q - \ddot{p}_{id}$.

A lot of optimization tools are capable of solving the constrained quadratic optimization problem in (33). However, most of the optimization methods may not be competent for real-time implementation. Thus, a one-layer RNN is employed to solve the optimization problem in (33) as follows [52]

$$\varepsilon_i^q \dot{\tau}_i^{q*} = -\nabla J_i^q(\tau_i^{q*}) - \frac{1}{\iota_i^q}\partial \sum_{k=1}^{N+N_o+2} \max\{0, \xi_{ik}^q\} \tag{34}$$

where $\varepsilon_i^q \in \mathbb{R}^+$ is a time constant. ι_i^q is a penalty parameter. $\xi_{i1}^q = \Psi_{i2}(Z_{i1})\tau_i^{q*} - b_{i1}$, $\xi_{ik}^q = -L_{g_i}L_{f_i}h_{ij}\tau_i^{q*} - b_{i2}$, $k = 2, \ldots, N$, $\xi_{ik}^q = -L_{g_i}L_{f_i}h_{io}\tau_i^{q*} - b_{i3}$, $k = N+1, \ldots, N+N_o$, $\xi_{i(N+N_o+1)}^q = \tau_i^{q*} - \bar{\tau}_i^{q*}$ and $\xi_{i(N+N_o+2)}^q = -\tau_i^{q*} + \underline{\tau}_i^{q*}$. $\partial\max\{0, \xi_{ik}^q\}$ is an exact penalty function expressed as

$$\partial\max\{0, \xi_{ik}^q\} = \begin{cases} \nabla\xi_{ik}^q, & \text{for } \xi_{ik}^q > 0, \\ [0,1]\nabla\xi_{ik}^q, & \text{for } \xi_{ik}^q = 0, \\ 0_2, & \text{for } \xi_{ik}^q < 0 \end{cases}$$

with [0, 1] is a set-valued map with image in the scope [0, 1]. By the literature [52], the neuronal state τ_i^{q*} of above RNN is exponentially convergent to the optimal solution in finite time.

Since $\tau_i^x = \tau_i^u\cos(\psi_i)$ and $\tau_i^y = \tau_i^u\sin(\psi_i)$, the optimal surge force τ_i^u and the desired yaw angle ψ_{ir} are given as

$$\begin{cases} \tau_i^u = \tau_i^x\cos(\psi_i) + \tau_i^y\sin(\psi_i), \\ \psi_{ir} = \text{atan2}\left(\tau_i^y, \tau_i^x\right), \end{cases} \tag{35}$$

where atan2$(\cdot)$ is a four quadrant inverse tangent function.

2) The Optimal Yaw Moment Controller: To obtain the time derivatives of ψ_{ir}, an RED-based nonlinear tracking differentiator (RED-basde NLTD) is presented as follows

$$\begin{cases} \dot{\Theta}_{i1} = -k_{i1}^{\Theta}\zeta_i^{\Theta\frac{1}{3}}\lceil\Theta_{i1} - \psi_{ir}\rfloor^{\frac{2}{3}} + \Theta_{i2}, \\ \dot{\Theta}_{i2} = -k_{i2}^{\Theta}\zeta_i^{\Theta\frac{2}{3}}\lceil\Theta_{i1} - \psi_{ir}\rfloor^{\frac{1}{3}} + \Theta_{i3}, \\ \dot{\Theta}_{i3} = -k_{i3}^{\Theta}\zeta_i^{\Theta}\text{sgn}(\Theta_{i1} - \psi_{ir}), \end{cases} \tag{36}$$

where Θ_{i1}, Θ_{i2} and Θ_{i3} represent the estimations of ψ_{ir}, $\dot{\psi}_{ir}$ and $\ddot{\psi}_{ir}$, respectively. k_{i1}^{Θ}, k_{i2}^{Θ} and k_{i3}^{Θ} are the positive designed constants. $\zeta_i^{\Theta} \in \mathbb{R}^+$ is a scaling factor.

Define the estimated errors $\tilde{\Theta}_{i1} = \Theta_{i1} - \psi_{ir}$, $\tilde{\Theta}_{i2} = \Theta_{i2} - \dot{\psi}_{ir}$ and $\tilde{\Theta}_{i3} = \Theta_{i3} - \ddot{\psi}_{ir}$. The time derivatives of $\tilde{\Theta}_{i1}$, $\tilde{\Theta}_{i2}$ and $\tilde{\Theta}_{i3}$ are inferred as follows

$$\begin{cases} \dot{\tilde{\Theta}}_{i1} = -k_{i1}^{\Theta}\zeta_i^{\Theta\frac{1}{3}}\lceil\tilde{\Theta}_{i1}\rfloor^{\frac{2}{3}} + \tilde{\Theta}_{i2}, \\ \dot{\tilde{\Theta}}_{i2} = -k_{i2}^{\Theta}\zeta_i^{\Theta\frac{2}{3}}\lceil\tilde{\Theta}_{i1}\rfloor^{\frac{1}{3}} + \tilde{\Theta}_{i3}, \\ \dot{\tilde{\Theta}}_{i3} = -k_{i3}^{\Theta}\zeta_i^{\Theta}\text{sgn}(\tilde{\Theta}_{i1}) - \psi_{ir}^{(3)}, \end{cases} \tag{37}$$

where $\psi_{ir}^{(3)}$ represents the time derivative of $\ddot{\psi}_{ir}$ satisfying $|\psi_{ir}^{(3)}| \le \bar{\psi}_{ir} \in \mathbb{R}^+$. According to Theorem 4 in [53], the error dynamics (37) are finite-time stable. Thus, it is also means that the estimation errors $\tilde{\Theta}_{i1}$, $\tilde{\Theta}_{i2}$ and $\tilde{\Theta}_{i3}$ are bounded and satisfied with $\|[\tilde{\Theta}_{i1}, \tilde{\Theta}_{i2}, \tilde{\Theta}_{i3}]\| \le \bar{\Theta}_i \in \mathbb{R}^+$.

To recover the unknown disturbance σ_i^r, an RED-based ESO is proposed as follows

$$\begin{cases} \dot{\hat{r}}_i = -k_{i1}^r\zeta_i^{r\frac{1}{2}}\lceil\hat{r}_i - r_i\rfloor^{\frac{1}{2}} + \hat{\sigma}_i^r + \tau_i^r/m_i^r, \\ \dot{\hat{\sigma}}_i^r = -k_{i2}^r\zeta_i^r\text{sgn}(\hat{r}_i - r_i), \end{cases} \tag{38}$$

where $\hat{r}_i$ and $\hat{\sigma}_i^r$ present the estimated values of r_i and σ_i^r, respectively. k_{i1}^r, $k_{i2}^r \in \mathbb{R}^+$ are the predefined observer gains. $\zeta_i^r \in \mathbb{R}^+$ is a scaling factor.

Letting $\tilde{r}_i = (\hat{r}_i - r_i)/\zeta_i^r$ and $\tilde{\sigma}_i^r = (\hat{\sigma}_i^r - \sigma_i^r)/\zeta_i^r$ the time derivatives of $\tilde{r}_i$ and $\tilde{\sigma}_i^r$ are presented as follows

$$\begin{cases} \dot{\tilde{r}}_i = -k_{i1}^r\lceil\tilde{r}_i\rfloor^{\frac{1}{2}} + \tilde{\sigma}_i^r, \\ \dot{\tilde{\sigma}}_i^r = -k_{i2}^r\text{sgn}(\tilde{r}_i) - \dot{\sigma}_i^r/\zeta_i^r. \end{cases} \tag{39}$$

Define a yaw tracking error $z_{i2} = \psi_i - \psi_{ir}$. The dynamic of z_{i2} along (12c)-(12d) and (35) can be deduced as follows

$$\dot{z}_{i2} = r_i - \dot{\psi}_{ir} \text{ and } \ddot{z}_{i2} = \sigma_i^r + \tau_i^r/m_i^r - \ddot{\psi}_{ir}. \tag{40}$$

To stabilize the error dynamic $\ddot{z}_{i2}$, a yaw control law is developed as follows

$$\tau_i^r = m_i^r\left(\ddot{\psi}_{ir} + \tau_i^{r*} - \hat{\sigma}_i^r\right), \tag{41}$$

where τ_i^{r*} is a optimal yaw moment.

Substituting (41) into (40), it has

$$\dot{z}_{i2} = r_i - \dot{\psi}_{ir} \text{ and } \ddot{z}_{i2} = -\tilde{\sigma}_i^r + \tau_i^{r*}. \tag{42}$$

To solve the optimal yaw moment τ_i^r, the following constraints are constructed to achieve the yaw stability.

Step 1. CLF-based stability constraint

To simplify the constraint design, the error dynamics (40) can be transformed as follows

$$\dot{Z}_{i2} = A_{i2}Z_{i2} + B_{i2}(-\tilde{\sigma}_i^r + \tau_i^{r*}), \tag{43}$$

where $Z_{i2} = [z_{i2}, \dot{z}_{i2}]^T$, $A_{i2} = [0, 1; 0, 0]$ and $B_{i2} = [0, 1]^T$.

To stabilize Z_{i2}, a Lyapunov function is developed as

$$V_{i2} = Z_{i2}^T P_{i2} Z_{i2}, \tag{44}$$

where P_{i2} is a positive definite matrix satisfying

$$A_{i2}^T P_{i2} + P_{i2}A_{i2} - \frac{P_{i2}B_{i2}B_{i2}^T P_{i2} - D_{i2}Q_{i2}D_{i2}}{\gamma_{i2}} = 0 \tag{45}$$

with $\gamma_{i2} \in \mathbb{R}^+$, $D_{i2} = \text{diag}\{1/\gamma_{i2}, 1\}$ and $Q_{i2} = Q_{i2}^T > 0$. $P_{i2} = D_{i2}P_{i2}'D_{i2}$ with $P_{i2}' = P_{i2}'^T > 0$ satisfying

$$A_{i2}^T P_{i2}' + P_{i2}'A_{i2} - P_{i2}'B_{i2}B_{i2}^T P_{i2}' + Q_{i2} = 0.$$

According to [51], the optimal yaw moment τ_i^{r*} should meet the following constraint:

$$\mathcal{U}_{i4} = \left\{\tau_i^{r*} : L_{A_{i2}}V_{i2} + L_{B_{i2}}V_{i2}\tau_i^{r*} + \frac{\epsilon_{i2}}{\gamma_{i2}}V_{i2} \le 0\right\}, \tag{46}$$

where $L_{A_{i2}}V_{i2} = Z_{i2}^T(P_{i2}A_{i2} + A_{i2}^T P_{i2})Z_{i2}$, $L_{B_{i2}}V_{i2} = 2Z_{i2}^T P_{i2}B_{i2}$ and $\epsilon_{i2} = \lambda_{\min}(Q_{i2})/\bar{\lambda}(P_{i2}')$.

To acquire the open-loop solution in $\mathcal{U}_{i4}$, a yaw pointwise min-norm control law is designed as follows

$$\tau_i^{r*} = \begin{cases} -\Psi_{i3}\Psi_{i4}/(\Psi_{i4}^T\Psi_{i4}), & \text{if } \Psi_{i3} > 0, \\ 0, & \text{if } \Psi_{i3} \le 0 \end{cases} \tag{47}$$

with $\Psi_{i3} = L_{A_{i2}}V_{i2} + \epsilon_{i2}V_{i2}/\gamma_{i2} + \varrho_{i2}\|L_{B_{i2}}V_{i2}\|$ and $\Psi_{i4} = L_{B_{i2}}V_{i2}$, where ϱ_{i2} is a positive constant.

Step 2. QP-based optimal yaw moment

To unify the yaw stability constraint (46) and input constraint, the optimal control input τ_i^{r*} is solved via the following quadratic optimization

$$\begin{aligned} \tau_i^{r*} = \ & \underset{\tau_i^{r*}\in\mathbb{R}}{\operatorname{argmin}} \ J_i^r(\tau_i^{r*}) = (\tau_i^{r*})^2 \\ \text{s.t.} \quad & \Psi_{i4}(Z_{i2})\tau_i^{r*} \leq -\Psi_{i3}(Z_{i2}), \\ & \underline{\tau}_i^{r*} \leq \tau_i^{r*} \leq \bar{\tau}_i^{r*}, \end{aligned} \tag{48}$$

where $\bar{\tau}_i^{r*} = \bar{\tau}_i^r/m_i^r - \ddot{\psi}_{ir} + \hat{\sigma}_i^r$ and $\underline{\tau}_i^{r*} = -\bar{\tau}_i^r/m_i^r - \ddot{\psi}_{ir} + \hat{\sigma}_i^r$.

In order to facilitate real-time implementation, a one-layer RNN is used to solve the QP problem as follows [52]

$$\varepsilon_i^r \dot{\tau}_i^{r*} = -\nabla J_i^r(\tau_i^{r*}) - \frac{1}{\iota_i^r}\partial \sum_{k=1}^{3} \max\{0, \xi_{ik}^r\} \tag{49}$$

where $\varepsilon_i^r \in \mathbb{R}^+$ is a time constant determining the convergence speed. ι_i^r is a penalty parameter. $\xi_{i1}^r = \Psi_{i4}(Z_{i2})\tau_i^{r*} + \Psi_{i3}(Z_{i2})$, $\xi_{i2}^r = \tau_i^{r*} - \bar{\tau}_i^{r*}$, $\xi_{i3}^r = -\tau_i^{r*} + \underline{\tau}_i^{r*}$. The function $\partial \max\{0, \xi_{ik}^r\}$ is an exact penalty function expressed as

$$\partial \max\{0, \xi_{ik}^r\} = \begin{cases} \nabla \xi_{ik}^r, & \text{for } \xi_{ik}^r > 0, \\ [0,1]\nabla \xi_{ik}^r, & \text{for } \xi_{ik}^r = 0, \\ 0_2, & \text{for } \xi_{ik}^r < 0. \end{cases}$$

It is proven in [52] that the state τ_i^{r*} of the RNN (49) can exponentially converge to the optimal solution in a finite time.

IV. Stability and Safety Analysis

This section analyzes the stability of the closed-loop system and the safety of the multi-ISV system.

A. Stability Analysis

To analyze the stability of RED-based ESO subsystems (18) and (39), the following assumption is needed.

Assumption 1: The time derivatives of σ_i^q and σ_i^r are bounded and satisfying $\|\dot{\sigma}_i^q\| \leq \bar{\sigma}_i^q$ and $|\dot{\sigma}_i^r| \leq \bar{\sigma}_i^r$ with $\bar{\sigma}_i^q, \bar{\sigma}_i^r$ being positive constants, respectively.

Letting $s_i^q = \operatorname{diag}\{|\tilde{q}_i^x|^{\frac{1}{2}}, |\tilde{q}_i^y|^{\frac{1}{2}}\}$ and $\varpi_i^q = -s_i^q\dot{\sigma}_i^q/\zeta_i^q$, it gets $\|\varpi_i^q\| \leq \bar{\sigma}_i^q\|s_i^q\|/\zeta_i^q$ and $\tilde{\varpi}_i^q = \bar{\sigma}_i^{q2}\|s_i^q\|^2/\zeta_i^{q2} - \|\varpi_i^q\|^2$. Define $Z_{i3} = [\lceil \tilde{q}_i \rfloor^{\frac{1}{2}}; \tilde{\sigma}_i^q]$, $S_i^q = \operatorname{diag}\{|\tilde{q}_i^x|^{\frac{1}{2}}, |\tilde{q}_i^y|^{\frac{1}{2}}, |\tilde{q}_i^x|^{\frac{1}{2}}, |\tilde{q}_i^y|^{\frac{1}{2}}\}$. Then, the error dynamics (18) can be rewritten as follows

$$\dot{Z}_{i3} = (S_i^q)^{-1}(A_{i3}Z_{i3} + B_{i3}\varpi_i^q), \tag{50}$$

where $A_{i3} = [-\frac{1}{2}k_{i1}^q I_2, \frac{1}{2}I_2; -k_{i2}^q I_2, 0_2]$ and $B_{i3} = [0_2; I_2]$.

Then, the stability of the RED-based ESO subsystem (17) is given via the following lemma.

Lemma 2: Under Assumption 1, the error dynamics of the RED-based ESO (17) can converge to the neighborhood origin in finite time, if there exists symmetric positive definite matrices P_{i3} and Q_{i3} such that

$$A_{i3}^T P_{i3} + P_{i3}A_{i3} + P_{i3}B_{i3}B_{i3}^T P_{i3} + C_{i1}^T C_{i1} = -Q_{i3} \tag{51}$$

with $C_{i1} = \bar{\sigma}_i^q[I_2, 0_2]$.

Proof: Consider a Lyapunov function candidate V_1 as $V_1 = Z_{i3}^T P_{i3} Z_{i3}$ Along (50), taking the time derivative of V_1 yields $\dot{V}_1 = Z_{i3}^T(A_{i3}^T(S_i^q)^{-1}P_{i3} + P_{i3}(S_i^q)^{-1}A_{i3})Z_{i3} + Z_{i3}^T P_{i3}(S_i^q)^{-1}B_{i3}\varpi_i^q + \varpi_i^{qT}B_{i3}^T(S_i^q)^{-1}P_{i3}Z_{i3} \leq \underline{\lambda}(S_i^q)(Z_{i3}^T(A_{i3}^T P_{i3} + P_{i3}A_{i3})Z_{i3} + Z_{i3}^T P_{i3}B_{i3}\varpi_i^q + \varpi_i^{qT}B_{i3}^T P_{i3}Z_{i3} + \|\tilde{\varpi}_i^q\|)$. From (51), $\dot{V}_1$ becomes $\dot{V}_1 \leq \underline{\lambda}(S_i^q)(Z_{i3}^T(A_{i3}^T P_{i3} + P_{i3}A_{i3} + C_{i1}^T C_{i1})Z_{i3} + Z_{i3}^T P_{i3}B_{i3}\varpi_i^q + (\varpi_i^q)^T B_{i3}^T P_{i3}Z_{i3} - \|\varpi_i^q\|^2) \leq -\underline{\lambda}(S_i^q)Z_{i3}^T Q_{i3}Z_{i3}$ and $\dot{V}_1 \leq -\underline{\lambda}(Q_{i3})\underline{\lambda}^{\frac{1}{2}}(P_{i3})/\bar{\lambda}(P_{i3})V_1^{\frac{1}{2}}$. According to [54], Z_{i3} converges to the origin in a finite time T satisfying $T \leq 2\bar{\lambda}(P_{i3})/(\underline{\lambda}(Q_{i3})\underline{\lambda}^{\frac{1}{2}}(P_{i3}))V_1^{\frac{1}{2}}(t_0)$.

Similarly, the stability of the RED-based ESO subsystem (39) is given by the following lemma without proof.

Lemma 3: Under Assumption 1, the error dynamics of the RED-based ESO (38) converge to the origin in a finite time, if there exists symmetric positive definite matrices P_{i4} and Q_{i4} such that $A_{i4}^T P_{i4} + P_{i4}A_{i4} + P_{i4}B_{i4}B_{i4}^T P_{i4} + C_{i2}^T C_{i2} = -Q_{i4}$, where $A_{i4} = [-k_{i1}^q/2, 1/2; -k_{i2}^q, 0]$, $B_{i4} = [0; 1]$, and $C_{i2} = [\bar{\sigma}_i^r, 0]$.

The following lemma shows the stability of the closed-loop system (22) and (43).

Lemma 4: Consider the closed-loop system (22) and (43). Under $\|\tilde{\sigma}_i^q\| \leq \bar{\sigma}_{ie}^q \in \mathbb{R}^+$ and $|\tilde{\sigma}_i^r| \leq \bar{\sigma}_{ie}^r \in \mathbb{R}^+$, the error signals of the closed-loop system are uniformly ultimately bounded with exponential convergence rate for all unknown disturbances σ_i^q and σ_i^r, and any $\psi_i(t_0)$ and $\nu_i(t_0)$.

Proof: Construct a Lyapunov function $V_2 = (V_{i1} + V_{i2})/2$. Taking the derivative of V_2 along (22) and (43), one has

$$\begin{aligned} \dot{V}_2 = \ & Z_{i1}^T P_{i1}A_{i1}Z_{i1} + Z_{i1}^T P_{i1}B_{i1}(-\tilde{\sigma}_i^q + \tau_i^{q*}) \\ & + Z_{i2}^T P_{i2}A_{i2}Z_{i2} + Z_{i2}^T P_{i2}B_{i2}(-\tilde{\sigma}_i^r + \tau_i^{r*}). \end{aligned} \tag{52}$$

According to (24) and (45), it renders that

$$\begin{aligned} \dot{V}_2 = \ & (Z_{i1}^T P_{i1}B_{i1}B_{i1}^T P_{i1}Z_{i1} - Z_{i1}^T D_{i1}Q_{i1}D_{i1}Z_{i1})/(2\gamma_{i1}) \\ & + (Z_{i2}^T P_{i2}B_{i2}B_{i2}^T P_{i2}Z_{i2} - Z_{i2}^T D_{i2}Q_{i2}D_{i2}Z_{i2})/(2\gamma_{i2}) \\ & + Z_{i1}^T P_{i1}B_{i1}(\tau_i^{q*} - \tilde{\sigma}_i^q) + Z_{i2}^T P_{i2}B_{i2}(\tau_i^{r*} - \tilde{\sigma}_i^r). \end{aligned} \tag{53}$$

Case I: $\Psi_{i1} > 0$ and $\Psi_{i3} > 0$:

By using the first conditions of (27) and (47), the equation (53) can be rewritten as $\dot{V}_2 = (Z_{i1}^T P_{i1}B_{i1}B_{i1}^T P_{i1}Z_{i1} - Z_{i1}^T D_{i1}Q_{i1}D_{i1}Z_{i1})/(2\gamma_{i1}) + (Z_{i2}^T P_{i2}B_{i2}B_{i2}^T P_{i2}Z_{i2} - Z_{i2}^T D_{i2}Q_{i2}D_{i2}Z_{i2})/(2\gamma_{i2}) - Z_{i1}^T(P_{i1}A_{i1} + A_{i1}^T P_{i1})Z_{i1}/2 - \varrho_{i1}\|Z_{i1}^T P_{i1}B_{i1}\| - Z_{i2}^T(P_{i2}A_{i2} + A_{i2}^T P_{i2})Z_{i2}/2 - \varrho_{i2}\|Z_{i2}^T P_{i2}B_{i2}\| - \epsilon_{i1}V_{i1}/(2\gamma_{i1}) - \epsilon_{i2}V_{i2}/(2\gamma_{i2}) - Z_{i1}^T P_{i1}B_{i1}\tilde{\sigma}_i^q - Z_{i2}^T P_{i2}B_{i2}\tilde{\sigma}_i^r$.

Based on (24) and (45), $\dot{V}_2$ can be deduced as $\dot{V}_2 = -Z_{i1}^T P_{i1}B_{i1}\tilde{\sigma}_i^q - \epsilon_{i1}V_{i1}/(2\gamma_{i1}) - \varrho_{i1}\|Z_{i1}^T P_{i1}B_{i1}\| - Z_{i2}^T P_{i2}B_{i2}\tilde{\sigma}_i^r - \epsilon_{i2}V_{i2}/(2\gamma_{i2}) - \varrho_{i2}\|Z_{i2}^T P_{i2}B_{i2}\|$. From Lemmas 2 and 3, $\tilde{\sigma}_i^q$ and $\tilde{\sigma}_i^r$ are bounded with $\|\tilde{\sigma}_i^q\| \leq \bar{\sigma}_{ie}^q$ and $|\tilde{\sigma}_i^r| \leq \bar{\sigma}_{ie}^r$. Thus, $\dot{V}_2$ can be represented as follow $\dot{V}_2 \leq -\epsilon_{i1}\underline{\lambda}(P_{i1})\|Z_{i1}\|/(2\gamma_{i1}) - \|Z_{i1}^T P_{i1}B_{i1}\|(\varrho_{i1} - \bar{\sigma}_{ie}^q) - \epsilon_{i2}\underline{\lambda}(P_{i2})\|Z_{i2}\|/(2\gamma_{i2}) - \|Z_{i2}^T P_{i2}B_{i2}\|(\varrho_{i2} - \bar{\sigma}_{ie}^r)$.

Case II: $\Psi_{i1} \leq 0$ and $\Psi_{i3} \leq 0$:

According to the definitions of Ψ_{i1} and Ψ_{i3}, it yields

$$\begin{cases} L_{A_{i1}}V_{i1} + \epsilon_{i1}V_{i1}/\gamma_{i1} + \varrho_{i1}\left\|2Z_{i1}^T P_{i1}B_{i1}\right\| < 0, & \text{(54a)} \\ L_{A_{i2}}V_{i2} + \epsilon_{i2}V_{i2}/\gamma_{i2} + \varrho_{i2}\left\|2Z_{i2}^T P_{i2}B_{i2}\right\| < 0. & \text{(54b)} \end{cases}$$

In this case, $\tau_i^{q*} = 0$ and $\tau_i^{r*} = 0$. Since the second and third terms of (54a) and (54b) are always positive, the negativeness of Ψ_{i1} and Ψ_{i3} stems from $L_{A_{i1}}V_{i1}$ and $L_{A_{i2}}V_{i2}$ to be negative and dominant, respectively. Thus, incorporating (24) and (45) can yield that $P_{i1}B_{i1}B_{i1}^TP_{i1} - D_{i1}Q_{i1}D_{i1} < 0$ and $P_{i2}B_{i2}B_{i2}^TP_{i2} - D_{i2}Q_{i2}D_{i2} < 0$. Then, it gets the positive definite matrices $H_{i1} = D_{i1}Q_{i1}D_{i1} - P_{i1}B_{i1}B_{i1}^TP_{i1}$ and $H_{i2} = D_{i2}Q_{i2}D_{i2} - P_{i2}B_{i2}B_{i2}^TP_{i2}$. With (24) and (45), one has $2P_{i1}A_{i1} = -H_{i1}/\gamma_{i1}$ and $2P_{i2}A_{i2} = -H_{i2}/\gamma_{i2}$. Substituting H_{i1} and H_{i2} into (52) has $\dot{V}_2 \leq -\underline{\lambda}(H_{i1})\|Z_{i1}\|/(2\gamma_{i1}) - \underline{\lambda}(H_{i2})\|Z_{i2}\|/(2\gamma_{i2}) + \|Z_{i1}^TP_{i1}B_{i1}\|\|\bar{\sigma}_{ie}^q\| + \|Z_{i2}^TP_{i2}B_{i2}\|\|\bar{\sigma}_{ie}^r\|$.

The two-sided stability analysis shows that the proposed system is uniformly ultimate bounded. The proof is completed.

B. Safety Analysis

The safety of the proposed multi-ISV system is given by the following lemma.

Lemma 5: Given an under-actuated ISV with dynamics (11), if the optimal control signal τ_i^{q*} belongs to $\mathcal{U}_{i2} \cap \mathcal{U}_{i3}$ for all ISVs, and $p_i(t_0) \in \mathcal{C}_{ij} \cap \mathcal{C}_{io}$, $\forall t > t_0$, $i = 1, \ldots, N$, the networked multi-ISV system is ISSf.

Proof: According to Lemma 1, the set $\mathcal{C}_{ij,1} \cap \mathcal{C}_{ij,2} \cap \mathcal{C}_{io,1} \cap \mathcal{C}_{io,2}$ is forward invariant by using the optimal control signal $\tau_i^{q*} \in \mathcal{U}_{i2} \cap \mathcal{U}_{i3}$, i.e. the set $\mathcal{C}_{ij} \cap \mathcal{C}_{io}$ is ISSF. It shows that if the initial position of all ISVs satisfies $p_i(t_0) \in \mathcal{C}_{ij} \cap \mathcal{C}_{io}$, $i = 1, \ldots, N$, $p_i(t)$ will always stay in $\mathcal{C}_{ij} \cap \mathcal{C}_{io}$. Therefore, the proposed multi-ISV system is ISSf.

The stability and safety of the proposed networked system of multiple ISVs are given by the following theorem.

Theorem 2: Consider a networked system of multiple ISVs with dynamics (11), the distributed motion generator (16), the RED-based ESOs (17) and (38), the stability constraints (26) and (46), the safety constraints (30) and (32), the NLTD (36), the optimal surge force (35) and the optimal yaw moment (49). All error signals of the proposed closed-loop system are uniformly ultimately bounded, and the multi-ISV system is ISSf; i.e. collision avoidance can be ensured.

Proof: According to Lemma 5, each ISV will not violate the safety requirements, i.e., the safety objective (14) and (15) are achieved. Lemma 4 shows that error signals Z_{i1} and Z_{i2} are bounded, and all tracking errors are ultimately bounded, i.e., there exists a positive constant μ such that the geometric objective (13) is achieved.

V. An Application to Vessel Train of Multiple ISVs

This section provides simulation results to verify the effectiveness of the proposed method. The proposed general safety-certified cooperative control architecture is applied to the control of vessel train system consisting of five interconnected ISVs numbered as 1-5 moving along a riverway. In addition, consider one obstructive ISV numbered as 6, one static obstacle numbered as 1 and one dynamic obstacle numbered as 2, shown in Fig. 4.

In order to achieve a fleet formation, each ISV is to track reference signals prescribed by the distributed motion generator (16) based on a consensus scheme as follows $\dot{p}_{1\,d} = q_{1\,d}$, $\dot{q}_{1\,d} = -l_1^2(p_{1\,d} - p_{0\,d} - d_{10}) - 2l_1q_{1\,d}$, $\dot{p}_{2\,d} = q_{2\,d}$, $\dot{q}_{2\,d} = -l_2^2(p_{2\,d} - p_{1\,d} - d_{21}) - 2l_2q_{2\,d}$, $\dot{p}_{3\,d} = q_{3\,d}$, $\dot{q}_{3\,d} = -l_3^2(p_{3\,d} - p_{2\,d} - d_{32}) - 2l_3q_{3\,d}$, $\dot{p}_{4\,d} = q_{4\,d}$, $\dot{q}_{4\,d} = -l_4^2(p_{4\,d} - p_{3\,d} - d_{43}) - 2l_4q_{4\,d}$, $\dot{p}_{5\,d} = q_{5\,d}$, $\dot{q}_{5\,d} = -l_5^2(p_{5\,d} - p_{0\,d} - d_{54}) - 2l_5q_{5\,d}$, where $p_{0\,d} = [t, 0.68t - 30]^T$, $l_1 = l_2 = l_3 = l_4 = l_5 = 2$ and $d_{10} = d_{21} = d_{32} = d_{43} = d_{54} = [-4.4721, -2.2361]^T$. Note that each ISV only communicates with its neighboring ISVs.

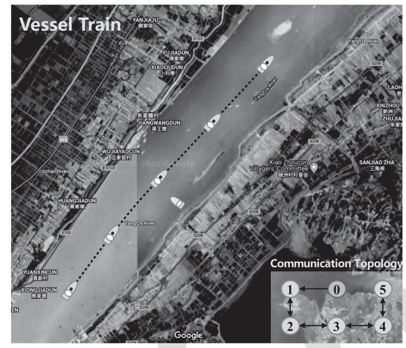

Fig. 4. An application to vessel train moving along a riverway.

In this simulation, the five ISVs are scaled-down vehicle model, and the model parameters can be found in [55]. The initial states of five ISVs and the obstructive ISV are set as $\eta_1(0) = [-10, -45, 2\pi/3]^T$, $\eta_2(0) = [-15, -48, 2\pi/3]^T$, $\eta_3(0) = [-20, -50, 2\pi/3]^T$, $\eta_4(0) = [-25, -52, 2\pi/3]^T$, $\eta_5(0) = [-30, -55, 2\pi/3]^T$, $\eta_6(0) = [140, 75, -\pi/2]^T$, $\nu_1(0) = \nu_2(0) = \nu_3(0) = \nu_4(0) = \nu_5(0) = [0, 0, 0]^T$ and $\nu_6(0) = [-0.075, -0.075, 0]^T$, respectively. The initial state of obstacles are set as $p_1(0) = [35, -10]^T$, $q_1(0) = [0, 0]^T$, $p_2(0) = [80, 38]^T$ and $q_2(0) = [0, -0.1]^T$, respectively. The radius of obstacles are assigned as $\rho_1 = 3$ and $\rho_2 = 2$. The safety parameters are selected as $R_c = 6$ and $R_o = 3$. In addition, parameters of the proposed safety-certified cooperative controller are selected as $k_{i1}^q = 2.12$, $k_{i2}^q = 1.1$, $\zeta_i^q = 3.5$, $k_{i1}^r = 2.12$, $k_{i2}^r = 1.1$, $\zeta_i^r = 3.5$, $k_{i1}^{\Theta} = 4$, $k_{i2}^{\Theta} = 5.6$, $k_{i3}^{\Theta} = 1.1$, $\zeta_i^q = 3.5$, $\epsilon_{i3} = 0.366$, $\gamma_{i1} = 4.0$, $\varrho_{i1} = 3.0$, $\epsilon_{i6} = 0.366$, $\gamma_{i2} = 0.5$, $\varrho_{i2} = 1.2$, $\kappa_{i1}(\chi_{ij,0}) = \chi_{ij,0}$, $\kappa_{i2}(\chi_{ij,1}) = \chi_{ij,1}$, $\kappa_{i1}(h_{io}) = h_{io}$, $\kappa_{i2}(\chi_{io}) = \chi_{io}$, $R_c = R_1 = R_2 = 2$, $l_i = 5$, $\varepsilon_i = 0.5$, $\iota_i = 1$.

Figs. 5– 9 show the simulation results. Specifically, Fig. 5 shows the trajectories of five ISVs and the reference trajectories generated by the distributed motion generator. It is seen that a vessel train formation can be achieved by using the proposed safety-certified controller (34) and (49) regardless of the dynamic obstacle, the static obstacle, and the obstructive ISV. Fig. 6 illustrates the collision avoidance process. Specifically, subfigure 6-(a) shows that there is no collision among neighboring ISVs during transient phase $0s \sim 50\,s$; subfigure 6-(b) shows that all ISVs can avoid the static obstacle during $50s \sim 100\,s$; subfigure 6-(c) implies that all ISVs can avoid the dynamic obstacle during $150s \sim 225\,s$; subfigure 6-(d) means that all ISVs can avoid the obstructive ISV during $250s \sim 300\,s$. These four subfigures demonstrate that the vessel train formation is safe during the whole sailing process. Fig. 7 depicts the earth-fixed tracking errors of five ISVs, and they exponentially converge to a small neighborhood of the origin. The four regions (a)-(d) in

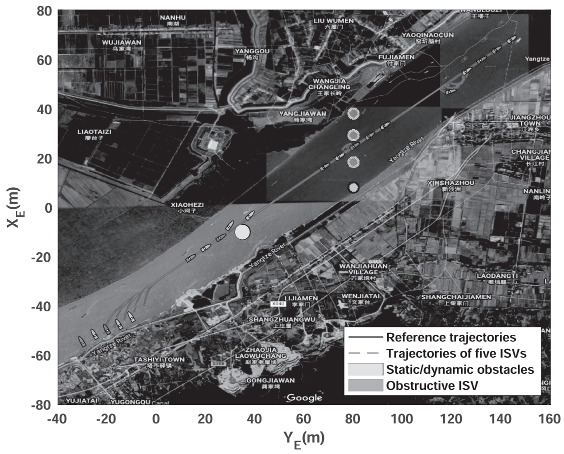

Fig. 5. The fleet trajectories of the five ISVs.

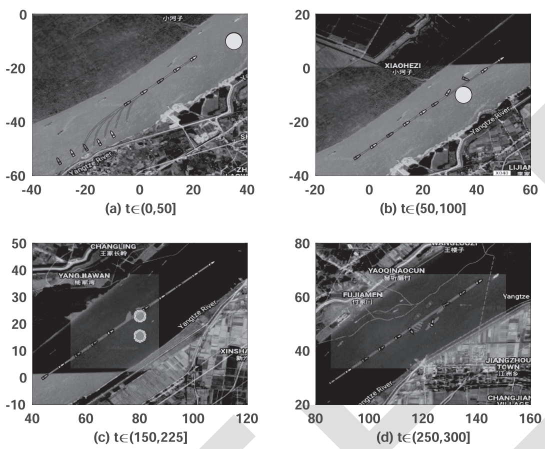

Fig. 6. The snapshots during different collision avoidance processes.

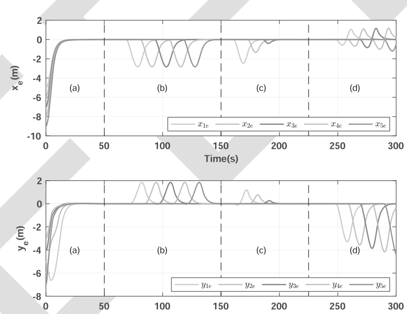

Fig. 7. Tracking errors of five ISVs. .

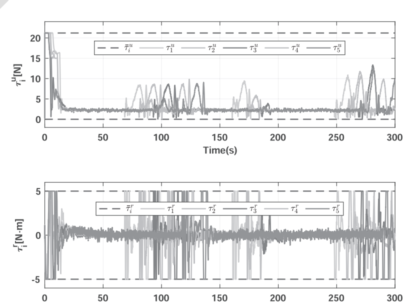

Fig. 8. The optimal surge force and yaw moment.

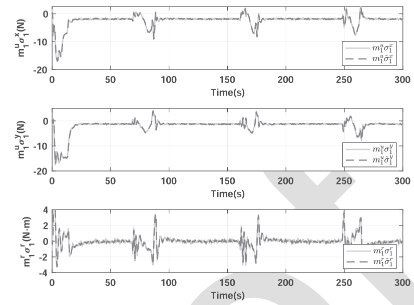

Fig. 9. The earth-fixed total disturbances.

Fig. 7 are consistent with the four subfigures in Fig. 6. It is also observed that the tracking errors become large because the safety objectives (14) and (15) take a higher priority than the geometric objective (13). Fig. 8 presents the optimal surge force and the optimal yaw moment within input constraints. The surge force and yaw moment tunes to satisfy the stability constraints (26) and (46), safety constraints (30) and (32) during the whole control process. Fig. 9 displays the estimation performance for the unknown total disturbances by using the proposed RED-based ESOs (17) and (38), and it can be seen that the total disturbance can be estimated accurately.

VI. Conclusion

This paper presents a general safety-certified cooperative control architecture for a fleet of under-actuated ISVs in the presence of multiple static/dynamic obstacles, in addition to model uncertainties, environmental disturbances, and input constraints. RED-based ESOs are designed for recovering unknown total disturbances in finite time. Based on CLF, ISSf-HOCBF and RED-based ESOs, optimal surge force and yaw moment are obtained by solving the constrained QPs subject to input, stability, safety constraints. One-layer RNNs are employed to solve the quadratic optimization problem on board, which enables real-time implementations without resorting to optimization tools. All tracking errors of the closed-loop system are proven to be uniformly ultimately bounded and the multi-ISV system is proven to be ISSf. Simulation results substantiate the effectiveness of the proposed general safety-certified cooperative control architecture.

References

[1] Z. Peng, J. Wang, D. Wang, and Q. Han, "An overview of recent advances in coordinated control of multiple autonomous surface vehicles," *IEEE Trans. Ind. Informat.*, vol. 17, no. 2, pp. 732–745, Feb. 2021.

[2] S. Xiao, X. Ge, Q.-L. Han, and Y. Zhang, "Resource-efficient platooning control of connected automated vehicles over VANETs," *IEEE Trans. Intell. Veh.*, to be published, doi: 10.1109/TIV.2022.3155640.

[3] X.-M. Zhang *et al.*, "Networked control systems: A survey of trends and techniques," *IEEE/CAA J. Automatica Sinica*, vol. 7, no. 1, pp. 1–17, Jan. 2020.

[4] I. Ahmad, X. Ge, and Q.-L. Han, "Communication-constrained active suspension control for networked in-wheel motor-driven electric vehicles with dynamic dampers," *IEEE Trans. Intell. Veh.*, to be published, doi: 10.1109/TIV.2022.3160165.

[5] X. Wang, "Active fault tolerant control for unmanned underwater vehicle with actuator fault and guaranteed transient performance," *IEEE Trans. Intell. Veh.*, vol. 6, no. 3, pp. 470–479, Sep. 2021.

[6] A. Vagale, R. Oucheikh, R. T. Bye, O. L. Osen, and T. I. Fossen, "Path planning and collision avoidance for autonomous surface vehicles I: A review," *J. Mar. Sci. Technol.*, vol. 26, pp. 1292–1306, 2021.

[7] J. Zhang, L. Pan, Q.-L. Han, C. Chen, S. Wen, and Y. Xiang, "Deep learning based attack detection for cyber-physical system cybersecurity: A survey," *IEEE/CAA J. Autom. Sinica*, vol. 9, no. 3, pp. 377–391, Mar. 2022.

[8] Z. Gao and G. Guo, "Command filtered finite/fixed-time heading tracking control of surface vehicles," *IEEE/CAA J. Autom. Sinica*, vol. 8, no. 10, pp. 1667–1676, Oct. 2021.

[9] K. D. Do, "Bounded controllers for formation stabilization of mobile agents with limited sensing ranges," *IEEE Trans. Autom. Control*, vol. 52, no. 3, pp. 569–576, Mar. 2007.

[10] Y. Dong and S. Xu, "A novel connectivity-preserving control design for rendezvous problem of networked uncertain nonlinear systems," *IEEE Trans. Neural Netw. Learn. Syst.*, vol. 31, no. 12, pp. 5127–5137, Dec. 2020.

[11] S. S. Ge, X. Liu, C. Goh, and L. Xu, "Formation tracking control of multiagents in constrained space," *IEEE Trans. Control Syst. Technol.*, vol. 24, no. 3, pp. 992–1003, May 2016.

[12] Z. Peng, J. Wang, and D. Wang, "Distributed maneuvering of autonomous surface vehicles based on neurodynamic optimization and fuzzy approximation," *IEEE Trans. Control Syst. Technol.*, vol. 26, no. 3, pp. 1083–1090, May 2018.

[13] W. Wu, Z. Peng, D. Wang, L. Liu, and N. Gu, "Anti-disturbance leader-follower synchronization control of marine vessels for underway replenishment based on robust exact differentiators," *Ocean Eng.*, vol. 248, 2022, Art. no. 110686.

[14] S. He, M. Wang, S. Dai, and F. Luo, "Leader-follower formation control of USVs with prescribed performance and collision avoidance," *IEEE Trans. Ind. Informat.*, vol. 15, no. 1, pp. 572–581, Jan. 2019.

[15] S.-L. Dai, S. He, H. Cai, and C. Yang, "Adaptive leader-follower formation control of underactuated surface vehicles with guaranteed performance," *IEEE Trans. Syst., Man, Cybern. Syst.*, vol. 52, no. 3, pp. 1997–2008, Mar. 2022.

[16] Z. Peng, D. Wang, T. Li, and M. Han, "Output-feedback cooperative formation maneuvering of autonomous surface vehicles with connectivity preservation and collision avoidance," *IEEE Trans. Cybern.*, vol. 50, no. 6, pp. 2527–2535, Jun. 2020.

[17] Z. Peng, L. Liu, and J. Wang, "Output-feedback flocking control of multiple autonomous surface vehicles based on data-driven adaptive extended state observers," *IEEE Trans. Cybern.*, vol. 51, no. 9, pp. 4611–4622, Sep. 2021.

[18] N. Gu, D. Wang, Z. Peng, and L. Liu, "Observer-based finite-time control for distributed path maneuvering of underactuated unmanned surface vehicles with collision avoidance and connectivity preservation," *IEEE Trans. Syst., Man, Cybern. Syst.*, vol. 51, no. 8, pp. 5105–5115, Aug. 2019.

[19] B. Wang, S. Nersesov, and H. Ashrafiuon, "Robust formation control and obstacle avoidance for heterogeneous underactuated surface vessel networks," *IEEE Trans. Control Netw. Syst.*, to be published, doi: 10.1109/TCNS.2022.3141022.

[20] G. Zhang, Y. Deng, and W. Zhang, "Robust neural path-following control for underactuated ships with the DVS obstacles avoidance guidance," *Ocean Eng.*, vol. 143, pp. 198–208, 2017.

[21] Q. Zhang, W. Pan, and V. Reppa, "Model-reference reinforcement learning for collision-free tracking control of autonomous surface vehicles," *IEEE Trans. Intell. Transp. Syst.*, to be published, doi: 10.1109/TITS.2021.3086033.

[22] B. S. Park and S. J. Yoo, "An error transformation approach for connectivity-preserving and collision-avoiding formation tracking of networked uncertain underactuated surface vessels," *IEEE Trans. Cybern.*, vol. 49, no. 8, pp. 2955–2966, Aug. 2018.

[23] B. S. Park and S. J. Yoo, "Connectivity-maintaining and collision-avoiding performance function approach for robust leader-follower formation control of multiple uncertain underactuated surface vessels," *Automatica*, vol. 127, 2021, Art. no. 109501.

[24] J. Ghommam, M. Saad, F. Mnif, and Q. M. Zhu, "Guaranteed performance design for formation tracking and collision avoidance of multiple USVs with disturbances and unmodeled dynamics," *IEEE Syst. J.*, vol. 15, no. 3, pp. 4346–4357, Sep. 2020.

[25] X. Sun and S. S. Ge, "Adaptive neural region tracking control of multi-fully actuated ocean surface vessels," *IEEE/CAA J. Autom. Sinica*, vol. 1, no. 1, pp. 77–83, Jan. 2014.

[26] K. D. Do, "Synchronization motion tracking control of multiple underactuated ships with collision avoidance," *IEEE Trans. Ind. Electron.*, vol. 63, no. 5, pp. 2976–2989, May 2016.

[27] Y. Cho, J. Kim, and J. Kim, "Intent inference-based ship collision avoidance in encounters with rule-violating vessels," *IEEE Robot. Automat. Lett.*, vol. 7, no. 1, pp. 518–525, Jan. 2022.

[28] Y. Jiang, Z. Peng, D. Wang, Y. Yin, and Q.-L. Han, "Cooperative target enclosing of ring-networked under-actuated autonomous surface vehicles based on data-driven fuzzy predictors and extended state observers," *IEEE Trans. Fuzzy Syst.*, to be published, doi: 10.1109/TFUZZ.2021.3087920.

[29] Y. Zhao, Y. Ma, and S. Hu, "USV formation and path-following control via deep reinforcement learning with random braking," *IEEE Trans. Neural Netw. Learn. Syst.*, vol. 32, no. 12, pp. 5468–5478, Dec. 2021.

[30] L. Ma, Y.-L. Wang, and Q.-L. Han, "Cooperative target tracking of multiple autonomous surface vehicles under switching interaction topologies," *IEEE/CAA J. Autom. Sinica*, to be published, doi: 10.1109/JAS.2022.105509.

[31] T. Li, R. Zhao, C. L. P. Chen, L. Fang, and C. Liu, "Finite-time formation control of under-actuated ships using nonlinear sliding mode control," *IEEE Trans. Cybern.*, vol. 48, no. 11, pp. 3243–3253, Nov. 2018.

[32] B. Liu, H.-T. Zhang, H. Meng, D. Fu, and H. Su, "Scanning-chain formation control for multiple unmanned surface vessels to pass through water channels," *IEEE Trans. Cybern.*, vol. 52, no. 3, pp. 1850–1861, Mar. 2022.

[33] Z. Peng, J. Wang, and D. Wang, "Containment maneuvering of marine surface vehicles with multiple parameterized paths via spatial-temporal decoupling," *IEEE/ASME Trans. Mechatronics*, vol. 22, no. 2, pp. 1026–1036, Apr. 2017.

[34] L. Liu, D. Wang, Z. Peng, and T. Li, "Modular adaptive control for LOS-based cooperative path maneuvering of multiple underactuated autonomous surface vehicles," *IEEE Trans. Syst., Man, Cybern. Syst.*, vol. 47, no. 7, pp. 1613–1624, Jul. 2017.

[35] Z. Peng, J. Wang, and D. Wang, "Distributed containment maneuvering of multiple marine vessels via neurodynamics-based output feedback," *IEEE Trans. Ind. Electron.*, vol. 64, no. 5, pp. 3831–3839, May 2017.

[36] Q. Zhang, L. Lapierre, and X. Xiang, "Distributed control of coordinated path tracking for networked nonholonomic mobile vehicles," *IEEE Trans. Ind. Informat.*, vol. 9, no. 1, pp. 472–484, Feb. 2013.

[37] N. Gu, Z. Peng, D. Wang, Y. Shi, and T. Wang, "Antidisturbance coordinated path following control of robotic autonomous surface vehicles: Theory and experiment," *IEEE/ASME Trans. Mechatronics*, vol. 24, no. 5, pp. 2386–2396, Oct. 2019.

[38] L. Qiao and W. Zhang, "Trajectory tracking control of AUVs via adaptive fast nonsingular integral terminal sliding mode control," *IEEE Trans. Ind. Informat.*, vol. 16, no. 2, pp. 1248–1258, Feb. 2020.

[39] L. Qiao and W. Zhang, "Double-loop integral terminal sliding mode tracking control for UUVs with adaptive dynamic compensation of uncertainties and disturbances," *IEEE J. Ocean. Eng.*, vol. 44, no. 1, pp. 29–53, Jan. 2019.

[40] L. Liu, D. Wang, and Z. Peng, "ESO-based line-of-sight guidance law for path following of underactuated marine surface vehicles with exact sideslip compensation," *IEEE J. Ocean. Eng.*, vol. 42, no. 2, pp. 477–487, Apr. 2017.

[41] S. Wang and J. Huang, "Cooperative output regulation of singular multi-agent systems under switching network by standard reduction," *IEEE Trans. Circuits Syst. I, Regular Papers*, vol. 65, no. 4, pp. 1377–1385, Apr. 2017.

[42] X. Ge, S. Xiao, Q.-L. Han, X.-M. Zhang, and D. Ding, "Dynamic event-triggered scheduling and platooning control co-design for automated vehicles over vehicular ad-hoc networks," *IEEE/CAA J. Autom. Sinica*, vol. 9, no. 1, pp. 31–46, Jan. 2021.

[43] Y. Huang, S. Z. Yong, and Y. Chen, "Stability control of autonomous ground vehicles using control-dependent barrier functions," *IEEE Trans. Intell. Veh.*, vol. 6, no. 4, pp. 699–710, Dec. 2021.

[44] S. Wang and J. Huang, "Adaptive leader-following consensus for multiple euler-lagrange systems with an uncertain leader system," *IEEE Trans. Neural Netw. Learn. Syst.*, vol. 30, no. 7, pp. 2188–2196, Jul. 2018.

[45] X. Ge, Q.-L. Han, J. Wang, and X.-M. Zhang, "A scalable adaptive approach to multi-vehicle formation control with obstacle avoidance," *IEEE/CAA J. Autom. Sinica*, to be published, doi: 10.1109/JAS.2021.1004263.

[46] Y. Chen, C. Hu, and J. Wang, "Motion planning with velocity prediction and composite nonlinear feedback tracking control for lane-change strategy of autonomous vehicles," *IEEE Trans. Intell. Veh.*, vol. 5, no. 1, pp. 63–74, Mar. 2019.

[47] W. Wu, Z. Peng, D. Wang, L. Liu, and Q.-L. Han, "Network-based line-of-sight path tracking of underactuated unmanned surface vehicles with experiment results," *IEEE Trans. Cybern.*, to be published, doi: 10.1109/TCYB.2021.3074396.

[48] R. Rout, R. Cui, and Z. Han, "Modified line-of-sight guidance law with adaptive neural network control of underactuated marine vehicles with state and input constraints," *IEEE Trans. Control Syst. Technol.*, vol. 28, no. 5, pp. 1902–1914, Sep. 2020.

[49] S. Kolathaya and A. D. Ames, "Input-to-state safety with control barrier functions," *IEEE Contr. Syst. Lett.*, vol. 3, no. 1, pp. 108–113, Jan. 2019.

[50] N. Gu, D. Wang, Z. Peng, J. Wang, and Q.-L. Han, "Disturbance observers and extended state observers for marine vehicles: A survey," *Control Eng. Pract.*, vol. 123, 2022, Art. no. 105158, doi: 10.1016/j.conengprac.2022.105158.

[51] A. D. Ames, K. Galloway, K. Sreenath, and J. W. Grizzle, "Rapidly exponentially stabilizing control lyapunov functions and hybrid zero dynamics," *IEEE Trans. Autom. Control*, vol. 59, no. 4, pp. 876–891, Apr. 2014.

[52] G. Li, Z. Yan, and J. Wang, "A one-layer recurrent neural network for constrained nonsmooth invex optimization," *Neural Netw.*, vol. 50, pp. 79–89, 2014.

[53] T. Sanchez, J. A. Moreno, and L. M. Fridman, "Output feedback continuous twisting algorithm," *Automatica*, vol. 96, pp. 298–305, 2018.

[54] Y. Hong, J. Huang, and Y. Xu, "On an output feedback finite-time stabilization problem," *IEEE Trans. Autom. Control*, vol. 46, no. 2, pp. 305–309, Feb. 2001.

[55] R. Skjetne, T. I. Fossen, and P. V. Kokotović, "Adaptive maneuvering, with experiments, for a model ship in a marine control laboratory," *Automatica*, vol. 41, no. 2, pp. 289–298, 2005.

Wentao Wu (Student Member, IEEE) received the B.E. degree in electrical engineering and automation from the Harbin University of Science and Technology, Harbin, China, in 2018 and the M.E. degree in electrical engineering from Dalian Maritime University, Dalian, China, in 2021. He is currently working toward the Ph.D. degree in electronic information from Shanghai Jiao Tong University, Shanghai, China. His research interests include guidance and control of unmanned surface vehicles.

Zhouhua Peng (Senior Member, IEEE) received the B.E. degree in electrical engineering and automation, the M.E. degree in power electronics and power drives, and the Ph.D. degree in control theory and control engineering from Dalian Maritime University, Dalian, China, in 2005, 2008, and 2011, respectively.

In December 2011, he joined the School of Marine Engineering, Dalian Maritime University, where he is currently a Professor with the School of Marine Electrical Engineering. From July 2014 to April 2018, he was a Postdoctoral Research Fellow with the School of Control Science and Engineering, Dalian University of Technology. From February 2016 to February 2018, he was a Hong Kong Scholar with the Department of Computer Science, City University of Hong Kong, Hong Kong. From January 2019 to February 2019 and from July 2019 to August 2019, he was a Senior Research Fellow with the Department of Computer Science, City University of Hong Kong. He is the author of more than 220 refereed publications. His research focuses on coordinated control of unmanned surface vehicles.

Prof. Peng was the recipient of the Science and Technology Award (First Class) from China Association of Oceanic Engineering in 2019, the natural science awards (Second Class) from Liaoning Province in 2013 and 2017, the Hong Kong Scholar Award in 2016, and the Science and Technology Award for Youth from China Institute of Navigation in 2017. He won the honor of the Young Talent in Science and Technology from the Ministry of Transport of the People's Republic of China in 2017, the Distinguished Young Talent in Science and Technology from Dalian in 2018, and the Bai-Qian-Wan Talent (level Bai) from Liaoning Province in 2019. He is an Associate Editor of the IEEE TRANSACTIONS ON SYSTEMS, MAN, AND CYBERNETICS: SYSTEMS. He also serves on the Editorial Board of the *Chinese Journal of Ship Research*, and the Early Career Advisory Board of IEEE/CAA JOURNAL OF AUTOMATICA SINICA.

Lu Liu (Member, IEEE) received the B.E. degree in electrical engineering and automation and the Ph.D. degree in marine electrical engineering from Dalian Maritime University, Dalian, China, in 2012 and 2018, respectively.

In 2018, she joined the School of Marine Engineering, Dalian Maritime University, where she is currently an Associate Professor with the School of Marine Electrical Engineering and a Postdoctoral Research Fellow with the School of Electrical Information and Electric Engineering, Shanghai Jiao Tong University, Shanghai, China. She has authored more than 40 refereed publications. Her research interests include guidance and control of single/multiple marine surface vehicles.

Dan Wang (Senior Member, IEEE) received the B.E. degree in industrial automation engineering from the Dalian University of Technology, Dalian, China, in 1982, the M.E. degree in marine automation engineering from Dalian Maritime University, Dalian, China, in 1987, and the Ph.D. degree in mechanical and automation engineering from The Chinese University of Hong Kong, Hong Kong, in 2001.

He is currently a Professor with the School of Marine Electrical Engineering, Dalian Maritime University. From November 2001 to October 2005, he was a Research Scientist with Temasek Laboratories, National University of Singapore, Singapore. From January 2012 to May 2012, he was a Visiting Professor with the Institute for Aerospace Studies, University of Toronto, Toronto, ON, Canada. He is the author of more than 260 refereed publications. His research interests include nonlinear system control theory, adaptive control, multiagent system control, and the applications in marine vehicles. Prof. Wang was the recipient of two natural science awards (Second Class) from the Government of Liaoning Province in 2013 and 2017, respectively, and the Science and Technology Award (First Class) from China Association of Oceanic Engineering in 2019. He has served on the committees of many IEEE sponsored conferences as the conference committee Co-Chair, Program Chair, and the Organizing Chair.